https://doi.org/10.5194/bg-2019-366
Preprint. Discussion started: 18 November 2019

Biogeosciences Discussions

Modelling the habitat preference of two key *Sphagnum* species in a poor fen as controlled by capitulum water retention

Jinnan Gong[1], Nigel Roulet[2], Steve Frolking[1,3], Heli Peltola[1], Anna M. Laine[1,4], Nicola Kokkonen[1], Eeva-Stiina Tuittila[1]

[1] School of Forest Sciences, University of Eastern Finland, P.O. Box 111, FI-80101 Joensuu, Finland

[2] Department of Geography, McGill University and Centre for Climate and Global Change Research, Burnside Hall, 805 rue Sherbrooke O., Montréal, Québec H3A 2K6

[3] Institute for the Study of Earth, Oceans, and Space, and Department of Earth Sciences, University of New Hampshire, Durham, NH 03824, USA

[4] Department of Ecology and Genetics, University of Oulu, P.O. Box 3000, FI-90014, Oulu, Finland

Abstract

Current peatland models generally lack dynamic feedback between the plant community structure and the environment, although the vegetation dynamics and ecosystem functioning are tightly linked. Realistic projections of peatland response to climate change requires including vegetation dynamics in ecosystem models. In peatlands, *Sphagnum* mosses are key engineers. The species composition in a moss community varies primarily following habitat moisture conditions. Hence, modelling the mechanisms in controlling the habitat preference of *Sphagna* is a good first step for modelling the community dynamics in peatlands. In this study, we developed the Peatland Moss Simulator (PMS), a process-based model, for simulating community dynamics of the peatland moss layer that results in habitat preferences of *Sphagnum* species along moisture gradients. PMS employed an individual-based approach to describe the variation of functional traits among shoots and the stochastic base of competition. At the shoot-level, growth and competition were driven by net photosynthesis, which was regulated by hydrological processes via capitulum water retention. The model was tested by predicting the habitat preferences of *S. magellanicum* and *S. fallax*, two key species representing dry (hummock) and wet (lawn) habitats in a poor fen peatland (Lakkasuo, Finland). PMS successfully captured the habitat preferences of the two *Sphagnum* species, based on observed variations in trait properties. Our model simulation further showed that the validity of PMS depended on the interspecific differences in capitulum water retention being correctly specified. Neglecting the water-retention differences led to the failure of PMS to predict the habitat preferences of the species in stochastic simulations. Our work highlights the importance of capitulum water retention to the dynamics and carbon functioning of *Sphagnum* communities in peatland ecosystems. Studies of peatland responses to changing environmental conditions thus

https://doi.org/10.5194/bg-2019-366
Preprint. Discussion started: 18 November 2019

need to include capitulum water processes as a control on the vegetation dynamics. For that our PMS model could be used as an elemental design for the future development of dynamic vegetation models for peatland ecosystems.

Keywords: *Sphagnum* moss; capitulum water content; competition; peatland community dynamics; process-based modelling; moss traits; Peatland Moss Simulator (PMS)

1.Introduction

Peatlands have important roles in the global carbon cycle as they store about 30% of the world's soil carbon (Gorham, 1991; Hugelius et al., 2013). Environmental changes, like climate warming and land-use changes, are expected to impact the carbon functioning of peatland ecosystems (Tahvanainen, 2011). Predicting the functioning of peatlands under environmental changes requires models to quantify the interactions among ecohydrological, ecophysiological and biogeochemical processes. These processes are known to be strongly regulated by vegetation (Riutta et al. 2007; Wu and Roulet, 2014), which can change during decadal timeframe under changing hydrological conditions (Tahvanainen, 2011). Current peatland models generally lack mechanisms for the dynamical feedbacks between vegetation and environment (e.g. Frolking et al., 2002; Wania et al., 2009). Therefore, those feedback mechanisms need to be identified and integrated with ecosystem processes, in order to support realistic predictions on peatland functioning and the research community working on global biogeochemical cycles.

A major fraction of peatland biomass is formed by *Sphagnum* mosses (Hayward and Clymo, 1983; Vitt, 2000). Although individual *Sphagnum* species often has narrow habitat niches (Johnson et al., 2015), different *Sphagnum* species replace each other along water-table gradient and therefore, as a genus, spread across a wide range of water table conditions (Andrus et al. 1986; Laine et al. 2009; Rydin and McDonald, 1985). The species composition of the *Sphagnum* community strongly affects ecosystem processes such as hydrology, carbon sequestration and peat formation (Clymo, 1970; O'Neill, 2000; Vitt, 2000; Turetsky, 2003). The production of biomass and litter from *Sphagna*, which gradually raises the moss carpet, in turn affects the species composition (Robroek et al. 2009). Hence, modelling the moss community dynamics is fundamental for predicting temporal changes of peatland vegetation. As the distribution of *Sphagnum* species primarily follows the variability in water level in a peatland community (Andrus 1986; Väliranta et al. 2007), modelling the habitat preference of *Sphagnum* species along a moisture gradient could be a good first step for predicting moss community dynamics in peatland ecosystems, based on "space-for-time" substitution (Blois et al., 2013).

For a given *Sphagnum* species, the preferable habitat represents the environmental conditions for it to achieve higher rates of net photosynthesis and shoot elongation than the peers (Robroek

https://doi.org/10.5194/bg-2019-366
Preprint. Discussion started: 18 November 2019

et al., 2007a; Keuper et al., 2011). Capitulum water content, which is determined by the balance between the evaporative loss and water gains from capillary rise and precipitation, represents one of the most important controls on net photosynthesis (Murray et al. 1989; Van Gaalen et al. 2007; Robroek et al., 2009). To quantify the water processes in mosses, hydrological models have been developed to simulate the water movement between moss carpet and the peat underneath (Price, 2008; Price and Waddington, 2010), as regulated by the variations in meteorological conditions and energy balance. On the other hand, experimental work has addressed the species-specific responses of net photosynthesis to changes in capitulum water content (Hájek and Beckett, 2008; Schipperges and Rydin, 2009) and light intensity (Rice et al., 2008; Laine et al., 2011; Bengtsson et al., 2016). Net photosynthesis and hydrological processes are linked via capitulum water retention, which controls the response of capitulum water content to water potential changes (Jassey & Signarbieux, 2019). However, these mechanisms have not been integrated with ecosystem processes in modelling. Due to the lack of quantitative tools, the hypothetical importance of capitulum water retention has not yet been verified.

Along with the need for quantifying the capitulum water processes, modelling the habitat preference of *Sphagna* needs to quantify the competition among mosses, which is referred to as the "race for space" (Robroek et al., 2007a; Keuper et al., 2011): *Sphagnum* shoots could form new capitula and spread laterally, if there is space available. This reduces or eliminates the light source for any plant that being covered underneath (Robroek et al. 2009). As the competition occur between neighboring shoots, its modelling requires downscaling water-energy processes from the ecosystem to the shoot level. For that, *Sphagnum* competition needs to be modelled as spatial processes, considering that spatial coexistence and the variations of functional traits among shoot individuals may impact the community dynamics (Bolker et al., 2003; Amarasekare, 2003). However, existing spatial-based models generally rely on simple coefficients to describe the interactions among individuals (e.g. Czárán and Iwasa, 1998; Anderson and Neuhauser, 2000; Gassmann et al., 2003; Boulangeat et al., 2018), thus being decoupled from environmental fluctuation or the stochasticity of biophysiological processes.

This study aims to develop and test a model, the Peatland Moss Simulator (PMS), to simulate community dynamics within peatland moss layer that results in realistic habitat preference of *Sphagnum* species along a moisture gradient. In PMS, *Sphagnum* photosynthesis is the central process driving community dynamics, and its competitiveness in the environment is controlled by the capitulum moisture content. The moisture content in turn is controlled by capitulum water retention and water balance. Therefore, we hypothesize that water retention of the capitula is the mechanism driving moss community dynamics. We test the model validity using data from an experiment based on two *Sphagnum* species with different position along moisture gradient in the same site. If our hypothesis holds, the model will (1) correctly predict the competitiveness of the two species in wet and dry habitats; and (2) fail to predict competitiveness if the capitulum water retention of the two species are not correctly specified.

https://doi.org/10.5194/bg-2019-366
Preprint. Discussion started: 18 November 2019

2. Materials and methods

2.1 Study site

The peatland site being modelled locates in Lakkasuo, Orivesi, Finland (61° 47' N; 24° 18' E). The site is a poor fen fed by mineral inflows from a nearby esker (Laine et al 2004). Most of the site is formed by lawns dominated by *Sphagnum recurvum* complex (*Sphagnum fallax*, accompanied by *Sphagnum flexuosum* and *Sphagnum angustifolium*) and *Sphagnum papillosum*. Less than 10% of surface are occupied by hummocks, which are 15-25 cm higher than the lawn surface with *Sphagnum magellanicum* and *Sphagnum fuscum.* Both microforms are covered by continuous *Sphagnum* carpet with sparse ground vascular canopies (projection cover of *Carex* 12% on average), which spread homogeneously over the topography. The annual mean water table was 15.6 ± 5.0 cm deep from lawn surface (Kokkonen et al., 2019). More information about the site can be found in Kokkonen et al. (2019).

2.2 Model outline

Peatland Moss Simulator (PMS) is a process-based, stochastic model, which simulates the temporal dynamics of *Sphagnum* community as driven by variations in water-energy conditions and individual-based interactions (Fig. 1). In PMS, the studied ecosystem is seen as a dual-column system consisted of hydrologically connected habitats of hummocks and lawns (community environment in Fig. 1). For each habitat type, the community area is downscaled to two-dimensional cells representing the scale of individual shoots (i.e. 1 cm^2). Each grid cell can be occupied by one capitulum from a single *Sphagnum* species. The community dynamics, i.e. the changes in species abundances, were driven by the growth and competition of *Sphagnum* shoots at the grid-cell level (Module I in Fig. 1). These processes were regulated by the grid-cell-specific conditions of water and energy (Module II in Fig. 1), which are derived from the community environment (Module III in Fig. 1).

In this study, we focused on developing Module I and II (Section 2.3) and employed an available soil-vegetation-atmosphere transport (SVAT) model (Gong et al., 2013a, 2016) to describe the water-energy processes for Module III (Appendix A). We assumed that the temporal variation in water-table was similar in lawns and hummocks, and the hummock-lawn differences in water table (*dWT* in Fig. 1) followed their difference in surface elevations (Wilson, 2012). At the grid cell level, the photosynthesis of capitula drove the biomass growth and elongation of shoots, which led to the "race for space" between adjacent grid cells. The net photosynthesis rate was controlled by capitulum water retention, which defines the responses of capitulum water content (W_{cap}) to water potential (h) changes (Section 2.4). The functional traits regulating the growth and competition processes were considered as random variables (Section 2.4). Unknown parameters that related

https://doi.org/10.5194/bg-2019-366
Preprint. Discussion started: 18 November 2019

146 the lateral water flows of the site are estimated using a machine-learning approach (Section 2.5).
147 Finally, Monte-Carlo simulation was used to support the analysis on the habitat preferences of
148 *Sphagnum* species and hypothesis tests (Section 2.6).

149

150

151

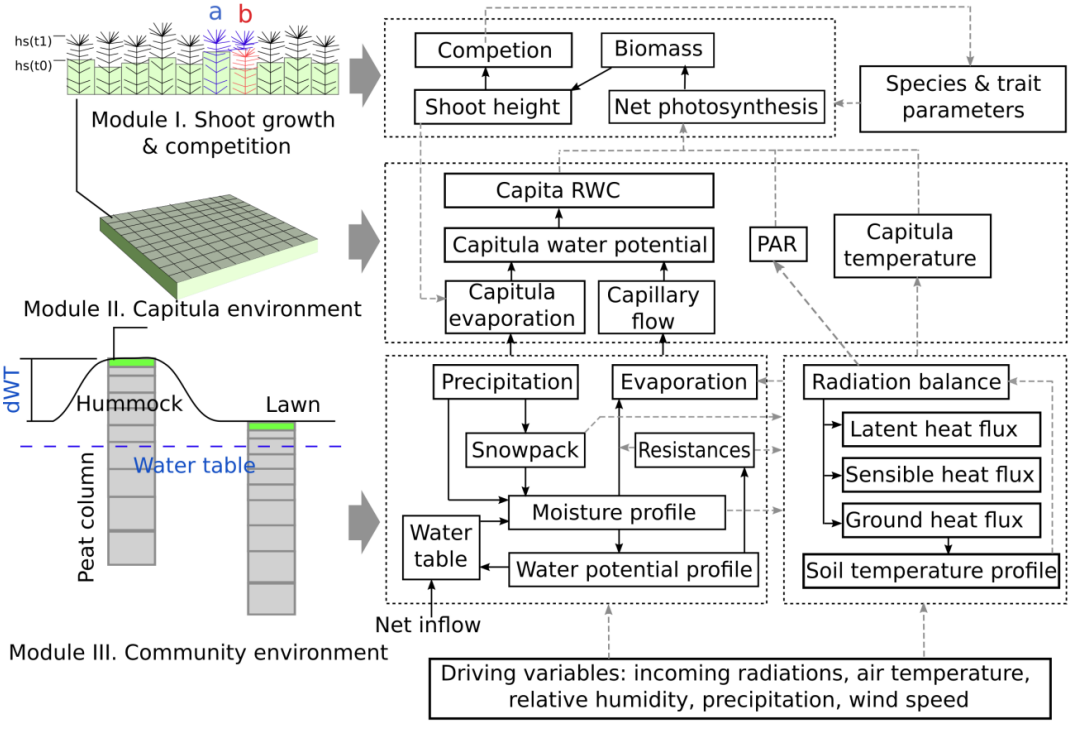

152

153 Fig. 1 Framework of Peatland Moss Simulator (PMS).

154

155 **2.3 Model development**

156 **2.3.1 Calculating shoot growth and competition of Sphagnum mosses (Module I)**

157 *Calculation of Sphagnum growth*

158 To model grid cell biomass production and height increment, we assumed that capitula were the
159 main parts of shoots responsible for photosynthesis and production of new tissues, instead of the
160 stem sections underneath. We employed a hyperbolic light-saturation function (Larcher, 2003) to
161 calculate the net photosynthesis, which was parameterized based on empirical measurements made

https://doi.org/10.5194/bg-2019-366
Preprint. Discussion started: 18 November 2019

from the target species collected from the study site (see Appendix B for materials and methods):

$$A_{20} = \left(\frac{Pm_{20} * PPFD}{\alpha_{PPFD} + PPFD} - Rs_{20}\right) * B_{cap} \quad (1)$$

where subscript 20 denotes the variable value measured at 20 °C; *Rs* is the mass-based respiration rate (μmol g^{-1} s^{-1}); *Pm* is the mass-based rate of maximal gross photosynthesis (μmol g^{-1} s^{-1}); *PPFD* is the photosynthetic photon flux density (μmol m^{-2} s^{-1}); and α_{PPFD} is the half-saturation point (μmol m^{-2} s^{-1}) for photosynthesis.

By adding multipliers for capitula water content (f_W) and temperature (f_T) to Eq. (1), the net photosynthesis rate *A* (μmol m^{-2} s^{-1}) was calculated as following:

$$A = \left[\frac{Pm_{20} * PPFD}{\alpha_{PPFD} + PPFD} f_T(T) - Rs_{20} f_R(T)\right] * B_{cap} * f_W(W_{cap}) \quad (2)$$

where $f_W(W_{cap})$ describes the responses of *A* to capitulum water content, W_{cap}; $f_T(T)$ describes the responses of *Pm* to capitulum temperature *T* (Korrensalo et al., 2017). $f_W(W_{cap})$ was estimated based on the empirical measurements (Appendix B; see Section 2.4). The temperature response $f_R(T)$ is a Q_{10} function that describes the temperature sensitivity of *Rs* (Frolking et al., 2002):

$$f_R(T) = Q_{10}^{(T - T_{opt})/10} \quad (3)$$

where Q_{10} is the sensitivity coefficient; *T* is the capitulum temperature (°C); T_{opt} (20 °C) is the reference temperature of respiration.

The response of *A* to W_{cap} ($f_W(W_{cap})$, Eq. 2) was described as a second-order polynomial function (Gong et al., 2019):

$$f_W(W_{cap}) = a_{W0} + a_{W1} * W_{cap} + a_{W2} * W_{cap}^2 \quad (4)$$

where a_{W0}, a_{W1} and a_{W2} are coefficients.

Plants can store carbohydrates as nonstructural carbon (NSC, e.g. starch and soluble sugar) to support fast growth in spring or post-stress periods, like after drought events (Smirnoff et al., 1992; Martínez-Vilalta et al., 2016; Hartmann and Trumbore, 2016). We linked the production of shoot biomass to the immobilization of NSC storage (modified from Eq. 10 in Asaeda and Karunaratne, 2000). The change in NSC storage depends on the balance between net photosynthesis and immobilization:

$$M_B = s_{imm} * NSC * k_{imm} \alpha_{imm}^{T-20} \quad (5)$$

$$\partial NSC / \partial t = A - M_B, NSC \epsilon [0, NSC_{max}] \quad (6)$$

where M_B is the immobilized NSC to biomass production during a time step (g); k_{imm} is the specific immobilization rate (g g^{-1}); α_{imm} is the temperature constant; s_{imm} is the multiplier for temperature threshold, where s_{imm} = 1 when T > 5 ºC but s_{imm} = 0 if $T \leq$ 5 ºC. NSC_{max} is the maximal NSC

https://doi.org/10.5194/bg-2019-366
Preprint. Discussion started: 18 November 2019

concentration in *Sphagnum* biomass (Turetsky et al., 2008).

The increase in shoot biomass drove the shoot elongation:

$$\partial Hc/\partial t = \frac{M_B}{H_{spc}S_c} \quad (7)$$

where Hc is the shoot height (cm); H_{spc} is the biomass density of *Sphagnum* stems (g m^{-2} cm^{-1}) and S_c is the area of a cell (m^2).

Calculation of Sphagnum competition and community dynamics

To simulate the competition among *Sphagnum* shoots, we first compared Hc of each grid cell (source grid cell, i.e. grid cell *a* in Fig. 1) to its four neighboring cells and marked the one with lowest position (e.g. grid cell *b* in Fig. 1) as the target of spreading. The spreading of shoots from a source to a target grid cell occurred when the following criteria were fulfilled: i) the height difference between source and target grid cells exceeded a threshold value; ii) the biomass accumulation in the source grid cell was large enough to support the growth of new capitula in the target grid cell; iii) the capitula in the source grid cell can split at most once per year.

The threshold of height difference in rule i) was set equal to the mean diameter of capitula in the source cell, based on the assumption that the shape of a capitulum was spherical. When shoots spread, the species type and model parameters in the target grid cell were overwritten by those in the source grid cell, assuming the mortality of shoots originally in the target cell. During the spreading, biomass and NSC storage were transferred from the source cell to the target cell to form new capitula. In case that the NSC storage in grid cell was exhausted, the metabolism of shoots became deactivated and the biomass growth or spreading stopped immediately. *Sphagnum* shoots in these deactivated grid cells could be re-established by invasion from neighboring cells. In cases where spreading did not take place, establishment of new shoots from spores was allowed to maintain the continuity of *Sphagnum* carpet at the site. During the establishment from spores, the type of *Sphagnum* species was randomized with moss parameters initialized as random numbers based on the measured means and variations.

2.3.2 Calculating grid cell-level dynamics of environmental factors (Module II)

Module II computes grid-cell values of W_{cap}, $PPFD$ and T for Module I. The cell-level $PPFD$ and T were assumed to be equal to the community means, which were solved by the SVAT scheme in Module III (Appendix A.). The community level evaporation rate (E) was partitioned to cell-level (E_i) as following:

$$E_i = E * \left(\frac{Sv_i}{r_{bulk,i}}\right) \Big/ \sum \left(\frac{Sv_i}{r_{bulk,i}}\right) \quad (8)$$

https://doi.org/10.5194/bg-2019-366
Preprint. Discussion started: 18 November 2019

where $r_{bulk,i}$ is the bulk surface resistance of cell i, which is as a function ($r_{bulk,i} = fr(h_i)$) of grid-cell-based water potential h_i, capitulum biomass (B_{cap}) and shoot density (D_S) based on the empirical measurements (Appendix B); Sv_i was the evaporative area, which was related to the height differences among adjacent grid cells:

$$Sv_i = Sc_i + lc \sum_j (Hc_i - Hc_j) \quad (9)$$

where lc is the width of a grid cell (cm); and subscript j denotes the four-nearest neighbouring grid cells. In this way, changes in the height difference between the neighboring shoots feeds back to affect the water conditions of the grid cells, via alteration of the evaporative surface area.

The grid cell-level changes in capitula water potential (h_i) was driven by the balance between the evaporation (E_i) and the capillary flow from the center of moss layer to capitula:

$$\partial h_i = \frac{K_m}{C_i}\left[\frac{(h_i - h_m)}{0.5 z_m} - 1 - E_i\right] \quad (10)$$

where h_m is the water potential of the living moss layer, solved in Module III (Appendix A.); z_m is the thickness of the living moss layer (z_m=5 cm); K_m is the hydraulic conductivity of the moss layer and that is set to be the same for each grid cell; C_i is the cell-level specific capacity of water ($C_i = \partial W_{cap,i}/\partial h_i$). $\partial W_{cap,i}/\partial h_i$ could be derived from the capitulum water retention function $h_i = f_h(W_{cap})$. W_{cap} can be then calculated from the estimated from h_i and affect the calculation of net photosynthesis through $f_W(W_{cap})$ (Eq. 2).

2.4 Model parameterization

Selection of Sphagnum species

We chose *S. fallax* and *S. magellanicum*, which form 63% of total plant cover at the study site at Lakkasuo (Kokkonen et al., 2019), as the target species representing the lawn and hummock habitats respectively. These species share similar a niche along the gradients of soil pH and nutrient richness (Wojtuń et al., 2003), but are discriminated by their preferences of water-table level (Laine et al., 2004). While *S. fallax* is commonly found close to the water table (Wojtuń et al., 2003), *S. magellanicum* can occur along a wider range of a dry-wet gradient, from intermediately wet lawns up to dry hummocks (Rice et al., 2008; Kyrkjeeide, et al., 2016; Korresalo et al., 2017). The transition from *S. fallax* to *S. magellanicum* along the wet-dry gradient thus indicates the decreasing competitiveness of *S. fallax* against *S. magellanicum* with a lowering water table.

Parameterization of morphological traits, net photosynthesis and capitulum water retention

We empirically quantified the morphological traits capitulum density (D_S, shoots cm^{-2}), biomass of capitula (B_{cap}, g m^{-2}), biomass density of living stems (H_{spc}, g cm^{-1} m^{-2}), net photosynthesis parameters (Pm_{20}, Rs_{20} and α_{PPFD}) and the water retention properties (i.e., $f_h(W_{cap})$ and $fr(h)$, Eqs.

https://doi.org/10.5194/bg-2019-366
Preprint. Discussion started: 18 November 2019

8 and 10) for the selected species from the same site (see Appendix B for methods). The values (mean ± SD) of the morphological parameters, the photosynthetic parameters and polynomial coefficients (a_{W0}, a_{W1} and a_{W2}, Eq. 3) are listed in Table. 1. For each parameter, a random value was initialized for each cell based on the measured means and SD, assuming the variation of parameter values is normally distributed.

We noticed that the fitted $f_W(W_{cap})$ was meaningful when $W_{cap} < W_{opt}$, which is the optimal water content for photosynthesis (W_{opt} = -0.5 a_{W1}/ a_{W2}). If $W_{cap} > W_{opt}$, photosynthesis decreased linearly with increasing W_{cap}, as being limited by the diffusion of CO_2 (Schipperges and Rydin, 1998). In that case, $f_W(W_{cap})$ was calculated following Frolking et al. (2002):

$$f_W(W_{cap}) = 1 - 0.5\frac{W_{cap}-W_{opt}}{W_{max}-W_{opt}} \quad (11)$$

where W_{max} is the maximum water content of capitula.

It is known that W_{max} is around 25-30 g g^{-1} (e.g. Schipperges and Rydin, 1998), or about 0.31 - 0.37 cm^3 cm^{-3} in term of volumetric water content (assuming 75 g m^{-2} capitula biomass and 0.6 cm height of capitula layer). This range is broadly lower than the saturated water content of moss carpet (> 0.9 cm^3 cm^{-3}, McCarter and Price, 2014). Consequently, we used the following equation to convert volumetric water content to capitula RWC, when h_i was higher than the boundary value of -10^4 cm:

$$W_{cap} = min(W_{max}, \theta_m/(H_{cap} * B_{cap} * 10^{-4})) \quad (12)$$

where W_{max} is the maximum water content that set to 25 g g^{-1}; θ_m is the volumetric water content of moss layer; H_{cap} is the height of capitula and is set to 0.6 cm (Hájek and Beckett, 2008).

Parameterization of SVAT processes

For the calculation of surface energy balance, we set the height and leaf area of vascular canopy to 0.4 m and 0.1 m^2 m^{-2}, consistent with the scarcity of vascular canopies at the site. The aerodynamic resistance (r_{aero}, Eq. A14, Appendix A) for surface energy fluxes was calculated following Gong et al. (2013a). The bulk surface resistance of community (r_{ss}, Eq. A13, Appendix A) was summarized from the cell-level values of $r_{bulk,i}$, that $1/r_{ss} = \sum(1/r_{bulk,i})$. To calculate the peat hydrology and water table, peat profiles of hummock and lawn communities were set to 150 cm deep and stratified into horizontal layers of depths varying from 5cm (topmost) to 30cm (deepest). For each peat layer, the thermal conductivity (K_T) of fractional components, i.e. peat, water and ice, were evaluated following Gong et al. (2013a). The bulk density of peat (ρ_{bulk}) was set to 0.06 g cm^{-3} below acrotelm (40 cm depth, Laine et al., 2004), and decreased linearly toward the living moss layer. The saturated hydraulic conductivity (K_{sat}, Eq. A6, Appendix A) and water retention parameters (i.e. α and *n*, Eq. A5, Appendix A) of water retention curves were calculated as functions of ρ_{bulk} and the depth of peat layer following Päivänen (1973). K_{sat}, α and *n* for the living moss layer were adopted from the values measured by McCarter and Price (2014) from *S.*

https://doi.org/10.5194/bg-2019-366
Preprint. Discussion started: 18 November 2019

magellanicum carpet. The parameter values for SVAT processes were listed in Table. 2.

Calculation of snow dynamics

We introduced a snow-pack model, SURFEX v7.2 (Vionnet et al., 2007), into the SVAT modelling. The snow-pack model simulates snow accumulation, wind drifting, compaction and changes in metamorphism and density. These processes influenced the heat transport and freezing-melting processes (i.e. S_h and S_T, see Eq. A1-A2, Appendix A). In this modelling, we calculate the snow dynamics on a daily basis in parallel to the SVAT simulation. Daily snowfall was converted into a snow layer and added to ground surface. For each of the day-based snow layers (D-layers), we calculated the changes in snow density, particle morphology and layer thicknesses. At each time step, D-layers were binned into layers of 5-10 cm depths (S-layers) and placed on top of the peat column for SVAT modelling. With a snow layer present, surface albedos (i.e. a_s, a_l) were modified to match those of the topmost snow layer (see Table. 4 in Vionnet et al., 2007). If the total thickness of snow was less than 5 cm, all D-layers were binned into one S-layer. The thermal conductivity (K_T), specific heat (C_T), snow density, thickness and water content of each S-layer were calculated as the mass-weighted means from the values of D-layers. Melting and refreezing tended to increase the density and K_T of a snow layer but decrease its thickness (see Eq. 18 in Vionnet et al., 2007). The fraction of melted water that exceeded the water holding capacity of a D-layer (see Eq. 19 in Vionnet et al., 2007) was removed immediately as infiltration water. If the peat layer underneath was saturated, the infiltration water was removed from the system as lateral discharge.

Boundary conditions and driving variables

A zero-flow boundary was set at the bottom of peat columns. The boundary conditions of water and energy at peat surface were defined by the ground surface temperature (T_0, see Eq. A10-A15 in Appendix A) and the net precipitation (P minus E). The profiles of layer thicknesses, ρ_{bulk} and hydraulic parameters were assumed to be constant during simulation. Periodic lateral boundary conditions were used to calculate the spreading of *Sphagnum* shoots among cells along the edge of the model domain.

The model simulation was driven by climatic variables of air temperature (*Ta*), precipitation (P), relative humidity (*Rh*), wind speed (*u*), incoming shortwave radiation (*Rs*) and longwave radiation (*Rl*). To support the stochastic parameterization of model and Monte-Carlo simulations, Weather Generator (Strandman et al., 1993) was used to generate randomized scenarios based on long-term weather statistics (period of 1981-2010) from 4 closest weather stations of Finnish Meteorological Institute. This generator had been intensively tested and applied under Finnish conditions (Kellomäki and Väisänen, 1997; Venäläinen et al., 2001; Alm et al., 2007). We also compared the simulated meteorological variables against 2-year data measured from Siikaneva peatland site (61°50 N; 24°10 E), located 10 km away from our study site (Appendix C).

https://doi.org/10.5194/bg-2019-366
Preprint. Discussion started: 18 November 2019

330

331 **2.5 Model calibration for lateral water influence**

332 We used a machine-learning approach to estimate the influence of upstream area on the water
333 balance of the site. The rate of net inflow (*I*, see Eq. A18 in Appendix A.) was described as a
334 function of Julian day (*JD*), assuming the inflow was maximum after spring thawing and then
335 decreased linearly with time:

336 $$I_j = (a_N * JD + b_N) * Ks_j, JD > JD_{thaw} \quad (11)$$

337 where subscript *j* denotes the peat layers under water table; *Ks* is the saturated hydraulic
338 conductivity; JD_{thaw} is the Julian day that thawing completed; and a_N and b_N are parameters.

339 We simulated water table changes using climatic scenarios from the Weather Generator (Section
340 2.4). During the calibration, the community compositions were set constant, that *S. magellanicum*
341 fully occupied the hummock habitat whereas *S. fallax* fully occupied the lawn habitat. The
342 simulated multi-year means of weekly water table values were compared to the mean water table
343 obtained observed at the site during years 2001, 2002, 2004 and 2016. The cost function for the
344 learning process was based on the sum of squared error (*SE*) of the simulated water table:

345 $$SE = \Sigma(WTs_k - WTm_k)^2 \quad (12)$$

346 where *WTm* is the measured multi-year mean of water table; *WTs* is the simulated multi-year mean
347 of water table; and subscript *k* denotes the week of year when the water table was sampled.

348 The values of a_N and b_N were estimated using the Gradient Descent approach (Ruder, 2016), by
349 minimizing *SE* in above Eq. (19):

350 $$X_N(j) := X_N(j) - \Gamma \frac{\partial SE}{\partial X_N(j)} \quad (13)$$

351 where Γ is the learning rate (Γ = 0.1). Appendix D shows the simulated water table with the
352 calibrated inflow term *I*, as compared against the measured values from the site.

353

354 **2.6 Model-based analysis**

355 First, we examined the ability of model to capture the preference of *S. magellanicum* for the
356 hummock environment and *S. fallax* for the lawn environment (Test 1). For both species, the
357 probability of occupation was initialized as 50% in a cell, and the distribution of species in the
358 communities were randomly patterned. Monte-Carlo simulations (40 replicates) were carried out,
359 with a time step of 30 minutes. A simulation length of 15 years was selected based on preliminary
360 studies, in order to cover the major part of change and ease the computational demand. Biomass
361 growth, stem elongation and the spreading of shoots were simulated on a daily basis. The
362 establishment of new shoots in deactivated cells was calculated at the end of each simulation year.

https://doi.org/10.5194/bg-2019-366
Preprint. Discussion started: 18 November 2019

We then assessed if the model could capture the dominance of *S. magellanicum* in the hummock communities and the dominance of *S. fallax* in lawn communities. The simulated annual height increments of mosses were compared to the values measured for each community type. To measure moss height growth, we deployed 20 cranked wires on *S. magellanicum* dominated hummocks and 15 on *S. fallax* dominated lawns in 2016. Each cranked wire was a piece of metal wire attached with plastic brushes at the side anchored into the moss carpet (e.g. Clymo 1970, Holmgren et al., 2015). Annual height growth (*dH*) was determined by measuring the change in the exposed wire length above moss surface from the beginning to the end of growing season.

Second, we tested the robustness of the model to the uncertainties in a set of parameters (Test 2). We focused on parameters that closely linked to hydrology and growth calculations, but were roughly parameterized (e.g. k_{imm}, r_{aero}) or adopted as a prior from other studies (e.g. K_{sat}, α, n, NSC_{max}; see Table. 2). One at a time, each parameter value was adjusted by +10 % or -10 %, and species cover was simulated using the same runtime settings as Test 1 with 40 Monte-Carlo runs. The simulated means of cover were then compared to those calculated without the parameter adjustment.

Tests 3-4 were then carried out to test whether the model could correctly predict competitiveness of the species in dry and wet habitats, if the species-specific trends of capitulum water retention were not correctly specified. For both species, we set the values of parameters controlling the water retention (Appendix B) and the water-stress effects on net photosynthesis (Eq. 4) to be the same as those in *S. magellanicum* (Test 3) or same as those in *S. fallax* (Test 4). Our hypothesis would be supported if removing the interspecific differences in *RWC* responses led to the failure to predict the habitat preferences of the species.

We implemented Tests 5-6 to test the importance of parameters that directly control the height increment (i.e. Pm_{20}, Rs_{20}, α_{PPFD} and H_{spec}) to the habitat preferences of the species. We eliminated the species differences in the parameter values to be same as those in *S. magellanicum* (Test 5) and same as those in *S. fallax* (Test 6). The effects of the manipulation on the simulated habitat preferences were compared against those from Tests 3-4. For each of Tests 3-6, 80 Monte-Carlo simulations were run using the setups described in Test 1.

3 Results

3.1 Simulating the habitat preferences of *Sphagnum* species as affected by water retention traits of capitulum

Test 1 showed the ability of model to capture the preference of *S. magellanicum* for the hummock environment and *S. fallax* for the lawn environment (Fig. 2A). The simulated annual changes in species covers were greater in lawn than in hummock habitats during the first 5 simulation years. The changes in lawn habitats slowed down around year 10 and the cover of *S. fallax* plateaued at

https://doi.org/10.5194/bg-2019-366
Preprint. Discussion started: 18 November 2019

399 around 95±2.8% (mean ±standard error). In contrast, the cover of *S. magellanicum* on hummocks
400 continued to grow until the end of simulation and reached 83±3.1%. In the lawn habitats, the cover
401 of *S. fallax* increased in all Monte-Carlo simulations and the species occupied all grid cells in 70%
402 of the simulations. In the hummock habitats, the cover of *S. magellanicum* increased in 91% of
403 Monte-Carlo simulations, and formed monocultural community in 16% of simulations (Fig. 2B).
404 The height growth of *Sphagnum* mosses was significantly greater at lawns than at hummocks
405 ($P<0.01$). The ranges of simulated height growths agreed well with the observed values from field
406 measurement for both species (Fig. 2C).

https://doi.org/10.5194/bg-2019-366
Preprint. Discussion started: 18 November 2019

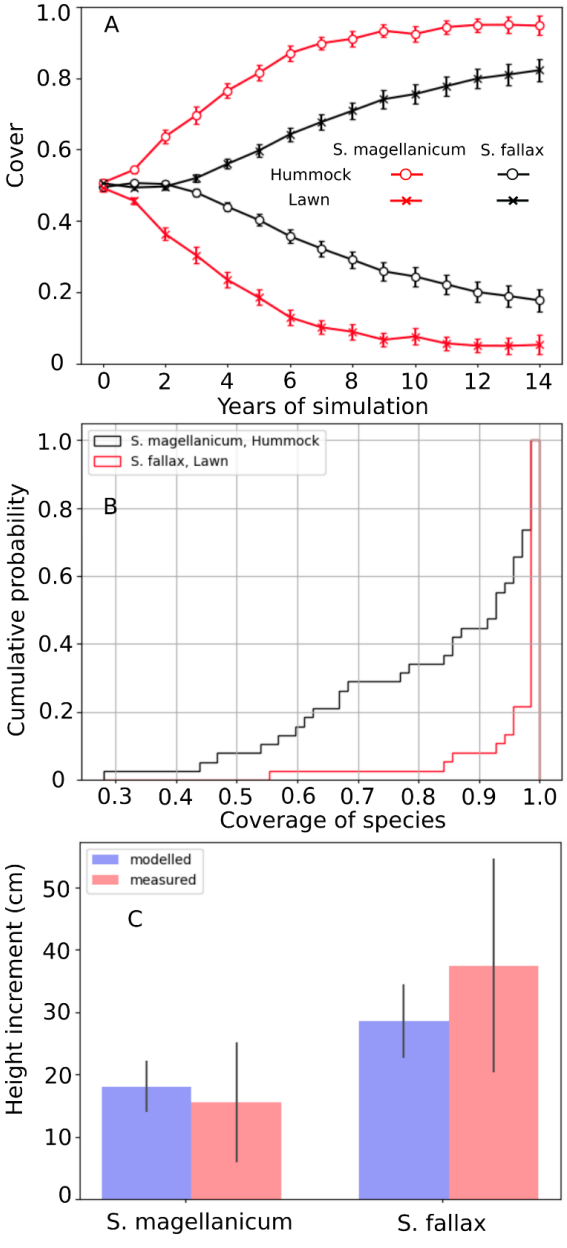

Figure 2. Testing the ability of PCS to predict habitat preference of *Sphagnum magellanicum* and *S. fallax* (Test 1). The hummock and lawn habitats were differentiated by water table depth, surface energy balances and capitulum water potential in modelling. In the beginning of simulation, the cover of the two species was set equal and it was allowed to develop with time. (A) Annual development of the cover (mean and standard error) of the two species in hummock and lawn habitats, (B) the cumulative probability distribution of the cover of the two species at the end of

https://doi.org/10.5194/bg-2019-366
Preprint. Discussion started: 18 November 2019

414 the 15-year period based on 80 Monte-Carlo simulations, and (C) the simulated and measured
415 means of annual height growth of *Sphagnum* surfaces in hummock and lawn habitats.

416

417 **3.2 Testing model robustness**

418 Test 2 addressed the model robustness to the uncertainties in several parameters that closely linked
419 to hydrology and growth calculations. Modifying most of the parameter values by +10% or -10%
420 yielded marginal changes in the mean cover of species in either hummock or hollow habitat (Table.
421 3). Reducing the moss carpet and peat hydraulic parameter *n* had stronger impacts on *S. fallax*
422 cover in hummocks than in lawns. Nevertheless, changes in simulated cover that were caused by
423 parameter manipulations were generally smaller than the standard deviations of the means.

424

425 **3.3 Testing the controlling role of capitulum water retention for community dynamics**

426 In Tests 3 and 4, the model incorrectly predicted the competitiveness of two species when the
427 interspecific differences of capitulum water retention were eliminated. In both tests, *S. fallax*
428 became dominant in all habitats. The use of water responses characteristic to *S. magellanicum* for
429 both species (Test 3) led to faster development of *S. fallax* cover and higher coverage at the end of
430 simulation (Fig. 3A), as compared with the simulation results where the water responses
431 characteristic to *S. fallax* were used for both species (Test 4, Fig. 3B). The pattern was more
432 pronounced in hummock than in lawn habitats.

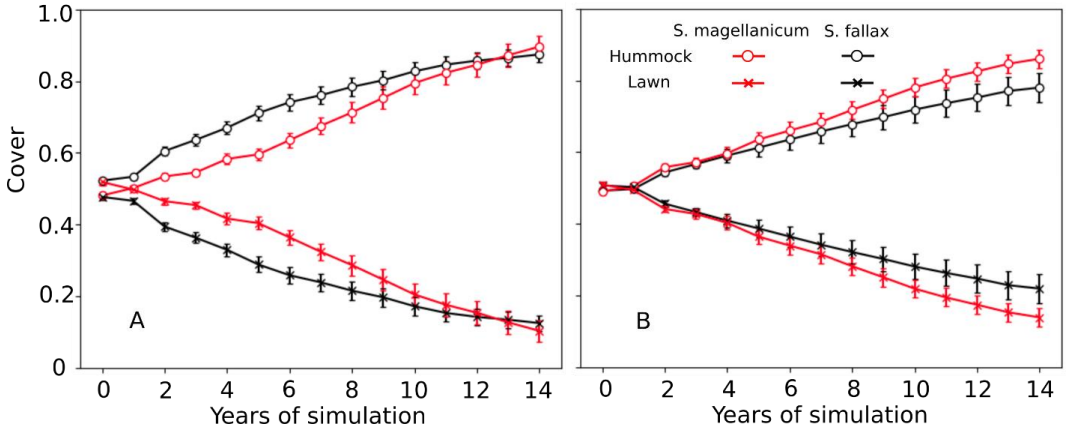

433 Figure 3. Testing the importance of capitulum water retention to the habitat preference of *S.*
434 *magellanicum* and *S. fallax*. The development of cover (mean and standard error) were simulated
435 in hummock and lawn habitats over a 15-year time frame for the two species. For both species,
436 parameter values for the capitulum water retention, capitulum biomass (B_{cap}) and density (D_S) were
437 set to be the same as those from (A) *S. magellanicum* (Test 3) or (B) *S. fallax* (Test 4).

https://doi.org/10.5194/bg-2019-366
Preprint. Discussion started: 18 November 2019

In Tests 5 and 6, the species differences in the growth-related parameters were eliminated. However, the model still predicted the dominances of *S. fallax* and *S. magellanicum* in lawn and hummock habitats, respectively (Fig. 4). The increase in the mean cover of *S. magellanicum* was especially fast in hummock habitat in comparison to the results of the unchanged model from Test 1 (Fig. 2A). In lawns, the use of *S. fallax* growth parameters for both species gave stronger competitiveness to *S. magellanicum* (Fig. 4B) than using the *S. magellanicum* parameters (Fig. 4A).

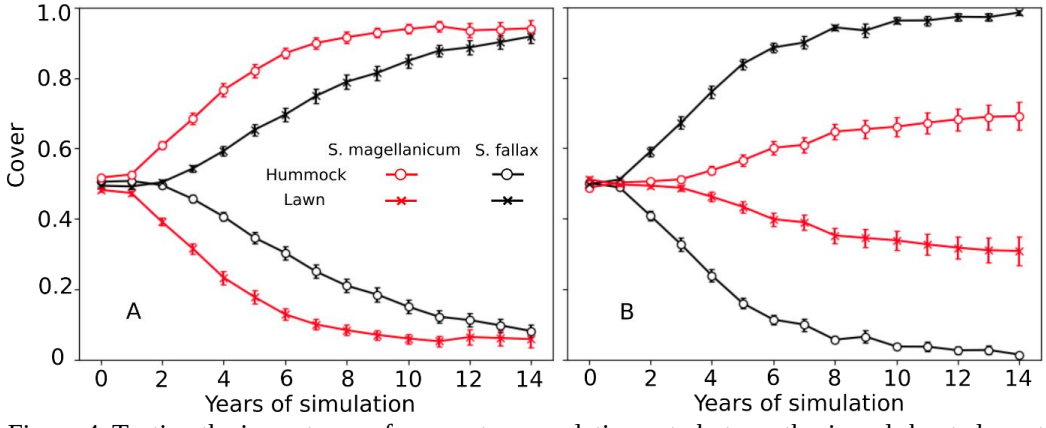

Figure 4. Testing the importance of parameters regulating net photosynthesis and shoot elongation to the habitat preference of *S. magellanicum* and *S. fallax*. Annual development of the cover (mean and standard error) of the two species were simulated for hummock and lawn habitats over a 15-year time frame. For both species, the parameter values (i.e. Pm_{20}, Rs_{20}, α_{PPFD} and H_{spec}) were set to be the same as those from (A) *S. magellanicum* (Test 5) or (B) *S. fallax* (Test 6).

4 Discussion

In peatland ecosystems, *Sphagnum* are keystone species differentially distributed primarily along the hydrological gradient. In a context where substantial change in peatland hydrology is expected under a changing climate in northern area (e.g. longer snow-free season, lower summer water table and more frequent droughts), there is a pressing need to understand how peatland plant communities could react and how *Sphagnum* species could redistribute under habitat changes. In this work, we developed Peatland Moss Simulator (PMS), a process-based stochastic model, to simulate the competition between *S. magellanicum* and *S. fallax*, two key species representing dry (hummock) and wet (lawn) habitats in a poor fen peatland. We empirically showed that these two species differed in characteristics that likely affect their competitiveness. The capitulum water retention for the lawn-preferring species (*S. fallax*) was weaker than that for the hummock-

https://doi.org/10.5194/bg-2019-366
Preprint. Discussion started: 18 November 2019

466 preferring species (*S. magellanicum*). Compared to *S. magellanicum*, the capitula of *S. fallax* held
467 less water at saturation and water content decreased more rapidly with dropping water potential.
468 Hence, *S. fallax* would dry faster than *S. magellanicum* under the same rate of water loss.
469 Moreover, the water content in *S. fallax* capitula was less resistant to evaporation. These
470 differences indicated that it is harder for *S. fallax* capitula to buffer evaporative loss of water and
471 thereby avoid or delay desiccation. In addition, the net photosynthesis of *S. fallax* is more sensitive
472 to changes in capitulum water content than *S. magellanicum*. Consequently, *S. fallax* is more likely
473 to be constrained by dry periods, when the capillary water cannot fully compensate the evaporative
474 loss (Robroek et al., 2007b) making it less competitive in habitats prone to desiccation. The PMS
475 successfully captured the habitat preferences of the two *Sphagnum* species (Test 1): starting from
476 a mixed community with equal probabilities for both species, the lawn habitats with shallower
477 water table were eventually dominated by the typical lawn species *S. fallax*, whereas hummock
478 habitats, which were 15 cm higher than the lawn surface, were taken over by *S. magellanicum*.
479 The low final cover of *S. magellanicum* simulated in lawn habitats agreed well with our
480 observation from the study site, where *S. magellanicum* cover was less than 1% over lawn
481 mesocosms (Kokkonen et al., 2019). On the other hand, *S. fallax* was outcompeted by *S.*
482 *magellanicum* in the hummock habitats. This result is consistent with previous findings that
483 hollow-preferring *Sphagna* are less likely to survive in hummock environments with greater
484 drought pressure (see Rydin 1985; Rydin et al. 2006; Johnson et al., 2015). The simulated annual
485 height increments of mosses also agreed well with the observed values for both habitat types. This
486 indicated that PMS can capture key mechanisms in controlling the growth and interactions of the
487 *Sphagnum* species.

488 The testing of parameter sensitivity showed the robustness of PMS regarding the uncertainties
489 in parameterization, as the simulated changes in the mean species cover were generally less than
490 the standard deviations of the means under 10% changes in several parameters. We found that
491 decreasing the value of hydraulic parameter *n* increased the presence of *S. fallax* in the hummock
492 habitats. This was expected: a lower *n* value will lead to higher water content in the unsaturated
493 layers (van Genuchten, 1978), which is important to wet-adapted *Sphagna* in order to survive dry
494 conditions (Hayward and Clymo, 1982; Robroek et al., 2007b; Rice et al., 2008). In contrast, the
495 response of *Sphagnum* cover to the changes in hydraulic parameters (i.e. α, n, K_h) were limited in
496 lawn habitats. This could be due to the relatively shallow water table in lawns, which was able to
497 maintain sufficient capillary rise to the moss carpet and capitula. Decreasing the values of k_{imm} and
498 NSC_{max} mainly decreased the cover of *S. fallax* in lawn habitats, consistent with the importance of
499 biomass production to *Sphagna* in high moisture environment (e.g. Rice et al., 2008; Laine et al.,
500 2011). In addition, the SVAT modelling for hummocks and lawns (Module III, Fig. 1) employed
501 same hydraulic parameter values obtained from *S. magellanicum* hummocks (McCarter and Price,
502 2014). This could overestimate K_m but underestimate n for lawns, as the lawn peat could be less
503 efficient in water retention and capillary-flow generation, as compared to hummock peat (Robroek

https://doi.org/10.5194/bg-2019-366
Preprint. Discussion started: 18 November 2019

et al., 2007b; Branham and Strack, 2014). As the decrease in K_m and increase in n showed counteracting effects on the simulated species covers (Table. 3), the biases in the parameterization of K_m and n may not critically impact model performance.

Both our empirical measurements and PMS simulations indicate the importance of capitulum water retention as a mechanism controlling the moss community dynamics in peatlands. On the one hand, our model predicted correctly the competitiveness of *S. magellanicum* against *S. fallax* in their preferred habitats, if the interspecific differences in water retention and water-stress effects were correctly specified (Test 1). Alternatively, the model failed to predict the distribution of *S. magellanicum* on hummocks, if these interspecific differences were neglected (Test 3 and Test 4, Fig. 3). This could be because the capillary rise during low water-table periods in summer may not fully compensate for the high evaporation (Robroek et al., 2007b; Nijp et al., 2014). In such circumstances, capitulum water potential could drop rapidly towards the pressure defined by the relative humidity of air (Hayward and Clymo, 1982). Consequently, the ability of capitula to retain cytoplasmic water would be particularly important for the hummock-preferring species. On the other hand, it is well acknowledged that a high growth rate is important to the competitiveness of *Sphagna* in habitats of high moisture content (Laing et al., 2014; Bengtsson et al., 2016). Our results also agreed on this, as setting the growth-related parameters (i.e. Pm_{20}, Rs_{20}, α_{PPFD} and H_{spec}) of *S. magellanicum* to be the same as those of *S. fallax* decreased the *S. fallax* cover in both hummock and lawn habitats (Test 6, Fig. 4B). However, the model still captured the habitat preferences for the tested species without including the interspecific differences in those growth-related parameters. Based on this, the growth-related parameters could be less important than those water-related ones.

There have been growing concerns on the shift of peatland communities from *Sphagnum*-dominant towards more vascular-abundant under a drier and warmer climate (Wullschleger et al., 2014; Munir et al. 2015; Dieleman et al. 2015). Nevertheless, the potential of *Sphagnum* species composition to adjust to this forcing remains poorly understood. Particularly in oligotrophic fens where the vegetation is substantially shaped by lateral hydrology (Tahvanainen, 2011; Turetsky et al., 2012), plant communities can be highly vulnerable to hydrological changes (Gunnarsson et al. 2002; Tahvanainen, 2011). Based on the validity and robustness of PMS, we believe PMS could serve as one of the first mechanistic tools to investigate the direction and rate of *Sphagnum* communities to change under environmental forcing. The hummock-lawn differences showed by Test 1 implied that *S. magellanicum* could outcompete *S. fallax* within a decadal time frame in a poor fen community, if the water table of habitats like lawns was lowered by 15 cm (Test 1). Although this was derived from a simplified system with only the two species, it highlighted the potential of rapid turnover of *Sphagnum* species: the hummock-lawn difference of water table in simulation was comparable to the expected water-table drawdown in fens under the warming climate (Whittington and Price, 2006; Gong et al., 2013b). Because of the large interspecific differences of traits such as photosynthetic potential, hydraulic properties and litter chemistry

https://doi.org/10.5194/bg-2019-366
Preprint. Discussion started: 18 November 2019

(Laiho 2006; Straková et al., 2011; Korrensalo et al., 2017; Jassey & Signarbieux, 2019), change in *Sphagnum* community composition is likely to impact long-term peatland stability and functioning (Waddington et al., 2015).

Although efforts have been made on analytical modelling to obtain boundary conditions for equilibrium states of moss and vascular communities in peatland ecosystems (Pastor et al., 2002), the dynamical process of peatland vegetation has not been well-described or included in earth system models (ESMs). Existing ecosystem models usually consider the features of peatland moss cover as "fixed" (Sato et al., 2007; Wania et al., 2009; Euskirchen et al., 2014), or change directionally following a projected trajectory (Wu and Roulet, 2014). Our modelling approach provided a way to incorporate the mechanisms of dynamical moss cover into peatland carbon modelling, and thus may serve the wider research community working on global biogeochemical cycles. PCS employed an individual-based approach where each grid cell carries a unique set of trait properties, so that shoots with favorable trait combinations in prevailing environment are thus able to replace those whose trait combinations are less favorable. This mimic the stochasticity in plant responses to environmental fluctuations, which are essential to community assembly and trait filtering under environmental forcing (Clark et al., 2010). Moreover, the model included the spatial interactions of individuals, which can impact the sensitivity of coexistence pattern to environmental changes (Bolker et al., 2003; Sato et al., 2007; Tatsumi et al., 2019). Because these features are essential to the "next generation" DVMs (Scheiter et al., 2013), PMS could be considered as an elemental design for future DVM development.

To conclude, our PMS could successfully capture the habitat preferences of the modelled *Sphagnum*. In this respect, our PMS model could provide fundamental support for the future development of dynamic vegetation models for peatland ecosystems. Based on our findings, the capitulum water processes should be considered as a control on the vegetation dynamics in future impact studies on peatlands under changing environmental conditions.

Acknowledgements
We are grateful to Harri Strandman (University of Eastern Finland) for the coding of Weather Generator. The project was funded by Academy of Finland (287039). AL acknowledges support from the Kone Foundation and SF from grant #1802825 from the US National Science Foundation, and the Fulbright-Finland and Saastamoinen Foundations.

Code and data availability. The data and the code to reproduce the analysis is available upon request to the corresponding author.

Author contributions. JG and EST designed the study. JG, AML and NK conducted the experiment and analysis. JG, EST, NR and SF designed the model. JG coded the model and conducted the

https://doi.org/10.5194/bg-2019-366
Preprint. Discussion started: 18 November 2019

model simulation and data analysis. JG wrote the manuscript with contributions from all co-authors.

Competing interests. The authors declare that they have no conflict of interest.

References

Alm, J., Shurpali, N. J., Tuittila, E.-S., Laurila, T., Maljanen, M., Saarnio, S. and Minkkinen, K.: Methods for determining emission factors for the use of peat and peatlands – flux measurements and modelling, Boreal Environment Research, 12, 85-100, 2007.

Amarasekare, P.: Competitive coexistence in spatially structured environments: A synthesis, Ecology Letters, 6, 1109-1122, 2003.

Anderson K. and Neuhauser C.: Patterns in spatial simulations—are they real? Ecological Modelling, 155, 19-30, 2000.

Andrus R. E.: Some aspects of Sphagnum ecology, Can. J. Bot., 64, 416–426, 1986.

Asaeda, T. and Karunaratne, S.: Dynamic modelling of the growth of Phragmites australis: model description, Aquatic Botany, 67, 301-318, 2000.

Bengtsson, F., Granath, G. and Rydin, H.: Photosynthesis, growth, and decay traits in Sphagnum - a multispecies comparison. Ecology and Evolution, 6, 3325-3341, 2016.

Blois, J. L., Williams, J. W., Fitzpatrick, M. C., Jackson, S. T. and Ferrier S.: Space can substitute for time in predicting climate-change effects on biodiversity, PNAS, 110, 9374-9379, doi:10.1073/pnas.1220228110, 2013.

Breeuwer, A., Heijmans, M. M., Robroek, B. J., Berendse, F. (2008). The effect of temperature on growth and competition between Sphagnum species. Oecologia, 156(1), 155-67.

Bolker, B. M., Pacala, S. W. and Neuhauser, C.: Spatial dynamics in model plant communities: What do we really know? Am. Nat., 162, 135–148, 2003.

Boulangeat, I., Svenning, J. C., Daufresne, T., Leblond, M. and Gravel, D.: The transient response of ecosystems to climate change is amplified by trophic interactions, Oikos, 127, 1822–1833, 2018.

Branham, J. E. and Strack, M.: Saturated hydraulic conductivity in *Sphagnum*-dominated peatlands: do microforms matter? Hydrol. Process., 28, 4352-4362, 2014.

Chesson, P. (2000). General theory of competitive coexistence in spatially varying environments. Theoretical Population Biology 58, 211–237.

Clapp, R. B., Hornberger, G. M. (1978). Empirical equations for some soil hydraulic properties.

https://doi.org/10.5194/bg-2019-366
Preprint. Discussion started: 18 November 2019

610 Water Resour. Res, 14, 601–604.

611 Clark J. S., Bell D., Chu C., Courbaud B., Dietze M., Hersh M., HilleRisLambers J., Ibanez I.,
612 LaDeau S., McMahon S., Metcalf, J., Mohan, J., Moran, E., Pangle, L., Pearson, S., Salk, C., Shen,
613 Z., Valle, D. and Wyckoff, P.: High-dimensional coexistence based on individual variation: a
614 synthesis of evidence, Ecological Monographs, 80, 569 – 608, 2010.

615 Clymo, R. S.: The growth of Sphagnum: Methods of measurement, Journal of Ecology, 58, 13-49,
616 1970.

617 Czárán T. and Iwasa Y.: Spatiotemporal models of population and community dynamics, Trends
618 Ecol. Evol., 13, 294–295, 1998.

619 Dieleman, C. M., Branfireun, B. A., Mclaughlin, J. W. and Lindo, Z.: Climate change drives a
620 shift in peatland ecosystem plant community: Implications for ecosystem function and stability,
621 Global Change Biology, 21, 388-395, 2015.

622 Euskirchen, E. S., Edgar, C. W., Turetsky, M. R., Waldrop, M. P. and Harden J. W.: Differential
623 response of carbon fluxes to climate in three peatland ecosystems that vary in the presence and
624 stability of permafrost, permafrost, J. Geophys. Res. Biogeosci., 119, 1576–1595, 2014.

625 Frolking, S., Roulet, N. T., Moore, T. R., Lafleur, T. M., Bubier, L. J. and Crill, P. M.: Modeling
626 seasonal to annual carbon balance of Mer Bleue Bog, Ontario, Canada. Global Biogeochem.
627 Cycles, 16, doi:10.1029/2001GB001457, 2002.

628 Gassmann, F., Klötzli, F. and Walther, G.: Simulation of observed types of dynamics of plants and
629 plant communities, Journal of Vegetation Science, 11, 397 – 408, 2003.

630 Goetz, J. D., Price, J. S. (2015). Role of morphological structure and layering of *Sphagnum* and
631 *Tomenthypnum* mosses on moss productivity and evaporation rates. Canadian Journal of Soil
632 Science, 95, 109-124.

633 Gong, J., Kokkonen, N., Laine, A. M. and Tuittila, E.-S.: Sphagnum capitula water retention as a
634 controlling mechanism for peatland moss community dynamics, Biogeosciences Discussion, bg-
635 2019-331, 2019 (submitted manuscript).

636 Gong, J., Shurpali, N., Kellomäki, S., Wang, K., Salam, M. M. and Martikainen, P. J.: High
637 sensitivity of peat moisture content to seasonal climate in a cutaway peatlandcultivated with a
638 perennial crop (Phalaris arundinacea, L.): a modeling study, Agricultural and Forest Meteorology,
639 180, 225–235, 2013a.

640 Gong, J., Wang, K., Kellomäki, S., Wang, K., Zhang, C., Martikainen, P. J. and Shurpali, N.:
641 Modeling water table changes in boreal peatlands of Finland under changing climate conditions,
642 Ecological Modelling, 244, 65-78, 2013b.

643 Gong, J., Jia, X., Zha, T., Wang, B., Kellomäki, S. and Peltola, H.: Modeling the effects of plant-

https://doi.org/10.5194/bg-2019-366
Preprint. Discussion started: 18 November 2019

644 interspace heterogeneity on water-energy balances in a semiarid ecosystem, Agricultural and
645 Forest Meteorology, 221, 189–206, 2016.

646 Gorham, E.: Northern peatlands: Role in the carbon cycle and probable responses to climatic
647 warming, Ecol. Appl., 1, 182–195, 1991.

648 Gunnarsson, U., Malmer, N. and Rydin, H.: Dynamics or constancy in Sphagnum dominated mire
649 ecosystems? A 40-year study, Ecography, 25, 685–704, 2002.

650 Hartmann, H. and Trumbore, S.: Understanding the roles of nonstructural carbohydrates in forest
651 trees – from what we can measure to what we want to know, New Phytol, 211, 386-403, 2016.

652 Hájek, T. and Beckett, R. P.: Effect of water content components on desiccation and recovery in
653 Sphagnum mosses, Annals of Botany, 101, 165–173, 2008.

654 Hájek, T., Tuittila, E.-S., Ilomets, M. and Laiho, R.: Light responses of mire mosses - A key to
655 survival after water-level drawdown? Oikos, 118, 240-250, 2009.

656 Hayward P. M. and Clymo R. S.: Profiles of water content and pore size in Sphagnum and peat,
657 and their relation to peat bog ecology. Proceedings of the Royal Society of London, Series B,
658 Biological Sciences, 215, 299-325, 1982.

659 Hayward P. M. and Clymo R. S.: The growth of Sphagnum: experiments on, and simulation of,
660 some effects of light flux and water-table depth. Journal of Ecology, 71, 845-863, 1983.

661 Holmgren, M., Lin, C., Murillo, J. E., Nieuwenhuis, A., Penninkhof, J., Sanders, N., Bart, T., Veen,
662 H., Vasander, H., Vollebregt, M. E. and Limpens, J.: Positive shrub–tree interactions facilitate
663 woody encroachment in boreal peatlands, J. Ecol., 103, 58-66, 2015.

664 Hugelius, G., Tarnocai, C., Broll, G., Canadell, J. G., Kuhry, P. and Swanson, D. K.: The Northern
665 Circumpolar Soil Carbon Database: spatially distributed datasets of soil coverage and soil carbon
666 storage in the northern permafrost regions, Earth Syst. Sci. Data, 5, 3-13, 2013.

667 Jassey, V. E., & Signarbieux, C.: Effects of climate warming on Sphagnum photosynthesis in
668 peatlands depend on peat moisture and species-specific anatomical traits. *Global change biology*,
669 *25*(11), 3859-3870, 2019.

670 Johnson, M. G., Granath, G., Tahvanainen, T., Pouliot, R., Stenøien, H. K., Rochefort, L., Rydin,
671 H. and Shaw, A. J.: Evolution of niche preference in Sphagnum peat mosses, Evolution, 69, 90 –
672 103, 2015.

673 Kellomäki, S. and Väisänen, H.: Modelling the dynamics of the forest ecosystem for climate
674 change studies in the boreal conditions, Ecol. Model., 97, 121-140, 1997.

675 Keuper, F., Dorrepaal, E., Van Bodegom, P. M., Aerts, R., Van Logtestijn, R. S.P., Callaghan, T.
676 V. and Cornelissen, J. H.C.: A Race for Space? How Sphagnum fuscum stabilizes vegetation
677 composition during long-term climate manipulations, Global Change Biology, 17, 2162–2171,

https://doi.org/10.5194/bg-2019-366
Preprint. Discussion started: 18 November 2019

678 2011.

679 Kokkonen, N., Laine, A., Laine, J., Vasander, H., Kurki, K., Gong, J. and Tuittila, E.-S.: Responses
680 of peatland vegetation to 15-year water level drawdown as mediated by fertility level. J. Veg. Sci.,
681 DOI: 10.1111/jvs.12794, 2019. (accepted manuscript)

682 Korrensalo, A., Alekseychik, P., Hájek, T., Rinne, J., Vesala, T., Mehtätalo, L., Mammarella, I.
683 and Tuittila, E.-S.: Species-specific temporal variation in photosynthesis as a moderator of
684 peatland carbon sequestration, Biogeosciences, 14, 257-269, 2017.

685 Kyrkjeeide, M. O., Hassel, K., Flatberg, K. I., Shaw, A. J., Yousefi, N. and Stenøien, H. K. Spatial
686 genetic structure of the abundant and widespread peatmoss Sphagnum magellanicum Brid. PLoS
687 One, 11, e0148447, 2016.

688 Laiho, R. Decomposition in peatlands: Reconciling seemingly contrasting results on the impacts
689 of lowered water levels, Soil Biology and Biochemistry, 38, 2011-2024, 2006.

690 Laine, A. M. Juurola, E., Hájek, T., Tuittila, E.-S. (2011). Sphagnum growth and ecophysiology
691 during mire succession. Oecologia, 167: 1115-1125.

692 Laine, J., Komulainen, V.-M., Laiho, R., Minkkinen, K., Ras- inm¨aki, A., Sallantaus, T.,
693 Sarkkola, S., Silvan, N., Tolonen, K., Tuittila, E.-S., Vasander, H., and Päivänen, J. (2004).
694 Lakkasuo – a guide to mire ecosystem, Department of Forest Ecology Publications, University of
695 Helsinki, 31, 123 pp.

696 Laine, J., Flatberg, K. I., Harju, P., Timonen, T., Minkkinen, K., Laine, A., Tuittila, E.-S.,
697 Vasander, H. (2018) Sphagnum Mosses — The Stars of European Mires. University of Helsinki
698 Department of Forest Sciences, Sphagna Ky. 326 p.

699 Laine J., Harju P., Timonen T., Laine A., Tuittila E.-S., Minkkinen K. and Vasander H.: The
700 inticate beauty of Sphagnum mosses—a Finnish guide to identification (Univ Helsinki Dept Forest
701 Ecol Publ 39). Department of Forest Ecology, University of Helsinki, Helsinki, pp 1–190, 2009.

702 Laing, C. G., Granath, G., Belyea, L. R., Allton K. E. and Rydin, H.: Tradeoffs and scaling of
703 functional traits in Sphagnum as drivers of carbon cycling in peatlands, Oikos, 123, 817–828,
704 2014.

705 Larcher, W.: Physiological Plant Ecology: Ecophysiology and Stress Physiology of Functional
706 Groups, Springer, 2003.

707 Letts, M. G., Roulet, N. T. and Comer, N. T.: Parametrization of peatland hydraulic properties for
708 the Canadian land surface scheme, Atmosphere-Ocean, 38, 141-160, 2000.

709 Martínez-Vilalta, J., Sala, A., Asensio, D., Galiano, L., Hoch, G., Palacio, S., Piper, F. I. and Lloret,
710 F.: Dynamics of non-structural carbohydrates in terrestrial plants: a global synthesis. Ecol Monogr,
711 86, 495-516, 2016.

https://doi.org/10.5194/bg-2019-366
Preprint. Discussion started: 18 November 2019

McCarter C. P. R. and Price J. S.: Ecohydrology of Sphagnum moss hummocks: mechanisms of capitula water supply and simulated effects of evaporation. Ecohydrology 7, 33 – 44, 2014.

Munir, T. M., Perkins, M., Kaing, E. and Strack, M.: Carbon dioxide flux and net primary production of a boreal treed bog: Responses to warming and water-table-lowering simulations of climate change, Biogeosciences, 12, 1091–1111, 2015.

Murray, K. J., Harley, P. C., Beyers, J., Walz, H. and Tenhunen, J. D.: Water content effects on photosynthetic response of Sphagnum mosses from the foothills of the Philip Smith Mountains, Alaska, Oecologia, 79, 244-250, 1989.

Nijp, J. J., Limpens, J., Metselaar, K., van der Zee, S. E. A. T. M., Berendse, F. and Robroek B. J. M.: Can frequent precipitation moderate the impact of drought on peatmoss carbon uptake in northern peatlands? New Phytologist, 203, 70-80, 2014.

O'Neill, K. P.: Role of bryophyte-dominated ecosystems in the global carbon budget. In A. J. Shaw and B. Goffi net [eds.] Bryophyte biology, 344–368, Cambridge University Press, Cambridge, UK, 2000.

Pastor, J., Peckham, B., Bridgham, S., Weltzin, J. and Chen J.: Plant community dynamics, nutrient cycling, and alternative stable equilibria in peatlands. American Naturalist, 160, 553-568, 2002.

Päivänen, J.: Hydraulic conductivity and water retention in peat soils, Acta Forestalia Fennica, 129, 1-69, 1973.

Pouliot, R., Rochefort, L., Karofeld, E., Mercier, C. (2011) Initiation of Sphagnum moss hummocks in bogs and the presence of vascular plants: Is there a link? Acta Oecologica, 37, 346-354.

Price, J. S., Whittington, P. N., Elrick, D. E., Strack, M., Brunet, N. and Faux, E.: A method to determine unsaturated hydraulic conductivity in living and undecomposed moss, Soil Sci. Soc. Am. J., 72, 487 – 491, 2008.

Price, J. S. and Whittington, P. N.: Water flow in Sphagnum hummocks: Mesocosm measurements and modelling, Journal of Hydrology 381, 333 – 340, 2010.

Rice, S. K., Aclander, L. and Hanson, D. T.: Do bryophyte shoot systems function like vascular plant leaves or canopies? Functional trait relationships in Sphagnum mosses (Sphagnaceae), American Journal of Botany, 95, 1366-1374, 2008.

Riutta, T., Laine, J., Aurela, M., Rinne, J., Vesala, T., Laurila, T., Haapanala, S., Pihlatie, M. and Tuittila, E.-S.: Spatial variation in plant community functions regulates carbon gas dynamics in a boreal fen ecosystem, Tellus, 59B, 838-852, 2007.

Robroek, B. J.M., Limpens, J., Breeuwer, A., Crushell, P. H. and Schouten, M. G.C.: Interspecific competition between Sphagnum mosses at different water tables, Functional Ecology, 21, 805 – 812, 2007a.

https://doi.org/10.5194/bg-2019-366
Preprint. Discussion started: 18 November 2019

747 Robroek, B. J.M., Limpens, J., Breeuwer, A., van Ruijven, J. and Schouten, M. G.C.: Precipitation
748 determines the persistence of hollow Sphagnum species on hummocks, Wetlands, 4, 979 – 986,
749 2007b.

750 Robroek, B. J.M., Schouten, M. G.C., Limpens, J., Berendse, F. and Poorter, H.: Interactive effects
751 of water table and precipitation on net CO_2 assimilation of three co-occurring Sphagnum mosses
752 differing in distribution above the water table, Global Change Biology 15, 680 – 691, 2009.

753 Ruder, S.: An overview of gradient descent optimization algorithms, CoRR, abs/1609.04747,
754 2016.

755 Runkle, B.R.K., Wille, C., Gažovič M., Wilmking, M. and Kutzbach, L.: The surface energy
756 balance and its drivers in a boreal peatland fen of northwestern Russia, Journal of Hydrology, 511,
757 359-373, 2014.

758 Rydin, H. and McDonald A. J. S.: Tolerance of Sphagnum to water level. Journal of Bryology, 13,
759 571–578, 1985.

760 Rydin, H., Gunnarsson, U., and Sundberg, S.: The role of Sphagnum in peatland development and
761 persistence, in: Boreal peatland ecosystems, edited by: Wieder, R. K., and Vitt, D. H.,30
762 Ecological Studies Series, Springer Verlag, Berlin, 47–65, 2006.

763 Sato, H., Itoh, A. and Kohyama, T.: SEIB-DGVM: A new Dynamic Global Vegetation Model
764 using a spatially explicit individual-based approach, Ecol. Model., 200, 279–307, 2007.

765 Scheiter, S., Langan, L. and Higgins, S. I.: Next-generation dynamic global vegetation models:
766 learning from community ecology, New Phytologist, 198, 957-969, 2013.

767 Schipperges, B. and Rydin, H.: Response of photosynthesis of Sphagnum species from contrasting
768 microhabitats to tissue water content and repeated desiccation, The New Phytologist, 140, 677-
769 684, 1998.

770 Silvola, J., Aaltonen, H. (1984) Water content and photo- synthesis in the peat mosses Sphagnum
771 fuscum and S. angustifolium. Annales Botanici Fennici 21, 1–6.

772 Smirnoff, N.: The carbohydrates of bryophytes in relation to desiccation tolerance, Journal of
773 Bryology, 17, 185-19, 1992.

774 Straková, P., Niemi, R. M., Freeman, C., Peltoniemi, K., Toberman, H., Heiskanen, I., Fritze, H.
775 and Laiho, R.: Litter type affects the activity of aerobic decomposers in a boreal peatland more
776 than site nutrient and water table regimes, Biogeosciences, 8, 2741-2755, 2011.

777 Strandman, H., Väisänen, H. and Kellomäki, S.: A procedure for generating synthetic weather
778 records in conjunction of climatic scenario for modelling of ecological impacts of changing climate
779 in boreal conditions, Ecol. Model., 70, 195–220, 1993.

780 Szurdoki, E., Márton, O., Szövényi, P. (2014): Genetic and morphological diversity of *Sphagnum*

https://doi.org/10.5194/bg-2019-366
Preprint. Discussion started: 18 November 2019

angustifolium, *S. flexuosum* and *S. fallax* in Europe. Taxon, 63: 237–48.

Tahvanainen, T.: Abrupt ombrotrophication of a boreal aapa mire triggered by hydrological disturbance in the catchment, Journal of Ecology, 99, 404-415, 2011.

Tatsumi, S., Cadotte M. W. and Mori, A. S.: Individual-based models of community assembly: Neighbourhood competition drives phylogenetic community structure, J. Ecol., 107, 735–746, 2019.

Thompson, D. K., Baisley, A. S. and Waddington, J. M.: Seasonal variation in albedo and radiation exchange between a burned and unburned forested peatland: implications for peatland evaporation, Hydrological Processes, 29, 3227-3235, 2015.

Turetsky, M. R.: The role of bryophytes in carbon and nitrogen cycling, Bryologist, 106, 395 – 409, 2003.

Turetsky, M. R., Crow, S. E., Evans, R. J., Vitt, D. H. and Wieder, R. K.: Trade-offs in resource allocation among moss species control decomposition in boreal peatlands, Journal of Ecology, 96, 1297-1305, 2008.

Turetsky, M. R., Bond-Lamberty, B., Euskirchen, E., Talbot, J., Frolking, S., McGuire, A. D. and Tuittila, E.: The resilience and functional role of moss in boreal and arctic ecosystems, New Phytologist, 196, 49-67, 2012.

van Gaalen, K. E., Flanagan, L. B., Peddle, D. R.: Photosynthesis, chlorophyll fluorescence and spectral reflectance in Sphagnum moss at varying water contents. Oecologia, 153, 19 – 28, 2007.

van Genuchten, M.: A closed-form equation for predicting the hydraulic conductivity of unsaturated soils, Soil Science Society of American Journal, 44, 892–898, 1980.

Väliranta, M., Korhola, A., Seppä, H., Tuittila, E. S., Sarmaja-Korjonen, K., Laine, J. and Alm, J.: High-resolution reconstruction of wetness dynamics in a southern boreal raised bog, Finland, during the late Holocene: a quantitative approach, The Holocene, 17, 1093–1107, 2007.

Venäläinen, A., Tuomenvirta, H., Lahtinen, R. and Heikinheimo, M.: The influence of climate warming on soil frost on snow-free surfaces in Finland, Climate Change, 50, 111-128, 2001.

Vionnet, V., Brun, E., Morin, S., Boone, A., Faroux, S., Le Moigne, P., Martin, E. and Willemet, J.-M.: The detailed snowpack scheme Crocus and its implementation in SURFEX v7.2, Geoscientific Model Development, 5, 773-791, 2012

Vitt, D. H.: Peatlands: Ecosystems dominated by bryophytes. In A. J. Shaw and B. Goffi net [eds.], Bryophyte biology, 312 – 343, Cambridge University Press, Cambridge, UK, 2000.

Waddington, J. M., Morris, P. J., Kettridge, N., Granath, G., Thompson, D. K. and Moore, P. A.: Hydrological feedbacks in northern peatlands, Ecohydrology, 8, 113 – 127, 2015.

Wania, R., Ross, I. and Prentice, I. C.: Integrating peatlands and permafrost into a dynamic global

https://doi.org/10.5194/bg-2019-366
Preprint. Discussion started: 18 November 2019

vegetation model: 2. Evaluation and sensitivity of vegetation and carbon cycle processes, Global Biogeochemical Cycles, 23, GB3015, DOI:10.1029/2008GB003413, 2009.

Weiss, R., Alm, J., Laiho, R. and Laine, J.: Modeling moisture retention in peat soils, Soil Science Society of America Journal, 62, 305–313, 1998.

Whittington, P. N. and Price, J. S.: The effects of water table draw-down (as a surrogate for climate change) on the hydrology of a fen peatland, Canada, Hydrological Processes, 20, 3589–3600, 2006.

Wilson, P. G.: The relationship among micro-topographic variation, water table depth and biogeochemistry in an ombrotrophic bog, Master Thesis, Department of Geography McGill University, Montreal, Quebec, p. 103, 2012.

Wojtuń B., Sendyk A. and Martynia, D.: Sphagnum species along environmental gradients in mires of the Sudety Mountains (SW Poland), Boreal Environment Research, 18, 74–88, 2003.

Wu, J. and Roulet, N. T.: Climate change reduces the capacity of northern peatlands to absorb the atmospheric carbon dioxide: The different responses of bogs and fens. Global Biogeochemical Cycles, doi.org/10.1002/2014GB004845, 2014.

Wullschleger, S. D., Epstein, H. E., Box, E. O., Euskirchen, E. S., Goswami, S., Iversen, C. M., Kattge, J., Norby, R. J., van Bodegom, P. M. and Xu, X.: Plant functional types in Earth system models: past experiences and future directions for application of dynamic vegetation models in high-latitude ecosystems, Ann. Bot., 114, 1–16, 2014.

https://doi.org/10.5194/bg-2019-366
Preprint. Discussion started: 18 November 2019

Biogeosciences Discussions Open Access EGU

Table. 1 Species-specific values of morphological and photosynthetic parameters for *S. magellanicum* and *S. fallax*. The parameters include: capitulum density (D_S, capitula cm^{-2}), capitulum biomass (B_{cap}, g m^{-2}), specific height of stem (H_{spc}, cm g^{-1} m^{-2}), maximal gross photosynthesis rate at 20 ºC (Pm_{20}, µmol g^{-1} s^{-1}), respiration rate at 20 ºC (Rs_{20}), half-saturation point of photosynthesis (α_{PPFD}, µmol g^{-1} s^{-1}), and polynomial coefficients (a_{W0}, a_{W1} and a_{W2}) for the responses of net photosynthesis to capitulum water content. Parameter values (mean ± standard deviation).

Parameter	*S. magellanicum*	*S. fallax*	Equation
D_S	0.922±0.289	1.46±0.323	-[a]
B_{cap}	75.4±21.5	69.2±19.6	-[a]
H_{spc}	45.4 ± 7.64	32.6±6.97	(7)
Pm_{20}	0.0189±0.00420	0.0140±0.00212	(2)
Rs_{20}	0.00729±0.00352	0.00651±0.00236	(2)
α_{PPFD}	101.4±14.1	143±51.2	(2)
a_{W0}	-1.354±0.623	-1.046±0.129	(4)
a_{W1}	0.431±0.197	0.755±0.128	(4)
a_{W2}	-0.0194±0.0119	-0.0751±0.0223	(4)

[a] the parameter was used in the linear models predicting the log_{10}-transformed capitulum water potential (h) and bulk resistance (r_{bulk}) for *S. fallax* and *S. magellanicum*. The function is detailed in Table 2 and Table 3 in Gong et al. (2019).

https://doi.org/10.5194/bg-2019-366
Preprint. Discussion started: 18 November 2019

847 Table. 2 Parameters values for SVAT simulations (Module III)

Parameter	Value	Equation	Source
Ksat	162	A6	McCarter and Price, 2014
n	1.43	A5	McCarter and Price, 2014
α	2.66	A5	McCarter and Price, 2014
θ_s	0.95[a]	A5	Päivänen, 1973
θ_r	0.071[b]	A5	Weiss et al., 1998
a_s	0.15	A9	Runkle et al., 2014
a_l	0.02	A10	Thompson et al., 2015
$K_{T,water}$	0.57	A4	Letts et al., 2000
$K_{T,ice}$	2.20	A4	Letts et al., 2000
$K_{T,org}$	0.25	A4	Letts et al., 2000
$C_{T,water}$	4.18	A3	Letts et al., 2000
$C_{T,ice}$	2.10	A3	Letts et al., 2000
$C_{T,org}$	1.92	A3	Letts et al., 2000
NSC_{max}	0.045	6	Turetsky et al., 2008

848 [a] The value was calculated from bulk density (ρ_{bulk}) as θ_s= 97.95 - 79.72ρ_{bulk} following Päivänen
849 (1973); [b] The value was calculated as θ_r = 4.3 + *67*ρ_{bulk} following Weiss et al. (1998).

https://doi.org/10.5194/bg-2019-366
Preprint. Discussion started: 18 November 2019

Biogeosciences Discussions Open Access EGU

Table. 3. Results from the test addressing the robustness of the model to the uncertainties in a set of parameters. Each parameter was increased or decreased by 10%. Model was run for *S. magellanicum* and *S. fallax* in their preferential habitats. Difference in mean cover between simulations under changed and unchanged parameter values are given with the standard deviations (SD) of the means in brackets.

Change in parameter value	Equation	Changes in simulated cover, % (SD)	
		S. magellanicum (hummock)	*S. fallax* (lawn)
kimm +10%	5	-1.2 (3.5)	-3.5 (3.8)
kimm -10%		+2.7 (0.4)	-5.0 (3.4)
NSC_{max} +10%	6	+4.5 (2.9)	+0.7 (3.0)
NSC_{max} -10%		-0.7 (4.0)	-4.8 (4.5)
K_m +10%	10	+1.0 (3.1)	-1.7 (2.3)
K_m -10%		-1.7 (2.7)	+4.1 (4.3)
K_h +10%	A1	-1.1 (3.0)	+1.1 (2.0)
K_h -10%		-1.8 (3.1)	-0.5 (2.7)
n +10%	A5	-1.6 (3.2)	-3.2 (3.2)
n -10%		-9.4 (3.6)	-0.3 (2.9)
α +10 %	A5	-0.5 (2.9)	-0.3 (2.3)
α -10 %		-1.3 (3.6)	+3.2 (1.0)
a_s +10%	A9	-2.2 (3.8)	+0.6 (2.1)
a_s -10%		+3.3 (3.4)	+1.2 (1.8)
r_{aero} +10%	A14, A15	-2.1 (3.4)	+0.3 (2.1)
r_{aero} -10%		-3.8 (4.4)	+2.3 (1.1)

https://doi.org/10.5194/bg-2019-366
Preprint. Discussion started: 18 November 2019

Appendix A. Calculating community SVAT scheme (Module III)

Transport of water and heat in peat profile

Simulating the transport of water and heat in the peat profiles was based on Gong et al. (2012, 2013). Here we list the key algorithms and parameters. Ordinary differential equations governing the vertical transport of water and heat in peat profiles were given as:

$$C_h \frac{\partial h}{\partial t} = \frac{\partial}{\partial z}\left[K_h\left(\frac{\partial h}{\partial z} + 1\right)\right] + S_h \quad \text{(A1)}$$

$$C_T \frac{\partial T}{\partial t} = \frac{\partial}{\partial z}\left(K_T \frac{\partial T}{\partial z}\right) + S_T \quad \text{(A2)}$$

where t is the time step; z is the thickness of peat layer; h is the water potential; T is the temperature; C_h and C_T are the specific capacity of water (i.e. $\partial\theta/\partial h$) and heat; K_h and K_T are the hydraulic conductivity and thermal conductivity, respectively; and S_h and S_T are the sink terms for water and energy, respectively.

C_T and K_T were calculated as the volume-weighted sums from components of water, ice and organic matter:

$$C_T = C_{water}\theta_{water} + C_{ice}\theta_{ice} + C_{org}(1 - \theta_{water} - \theta_{ice}) \quad \text{(A3)}$$

$$K_T = K_{water}\theta_{water} + K_{ice}\theta_{ice} + K_{org}(1 - \theta_{water} - \theta_{ice}) \quad \text{(A4)}$$

where C_{water}, C_{ice} and C_{org} are the specific heats of water, ice and organic matter, respectively; K_{water}, K_{ice} and K_{org} are the thermal conductivities of water, ice and organic matter, respectively; and θ_{water} and θ_{ice} are the volumetric contents of water and ice, respectively.

For a given h, $C_h = \partial\theta(h)/\partial h$ was derived from the van Genuchten water retention model (van Genuchten, 1980) as:

$$\theta(h) = \theta_r + \frac{(\theta_s - \theta_r)}{[1 + (\alpha|h^n|)^m]} \quad \text{(A5)}$$

where θ_s is the saturated water content; θ_r is the permanent wilting point water content; α is a scale parameter inversely proportional to mean pore diameter; n is a shape parameter; and m=1-1/n.

Hydraulic conductivity (K_h) in an unsaturated peat layer was calculated as a function of θ by combining the van Genuchten model with the Mualem model (Mualem, 1976):

$$K_h(\theta) = K_{sat} S_e^{L_e}\left[1 - \left(1 - S_e^{1/m}\right)^m\right] \quad \text{(A6)}$$

where K_{sat} is the saturated hydraulic conductivity; S_e is the saturation ratio and $S_e = (\theta - \theta_r)/(\theta_s - \theta_r)$; and L_e is the shape parameter (L_e=0.5; Mualem, 1976).

Boundary conditions and surface energy balance

A zero-flow condition was assumed at the lower boundary of the peat column. The upper boundary condition was defined by the surface energy balance, which was driven by net radiation (Rn). The dynamics of Rn at surface x (x=0 for vascular canopy and x=1 for moss surface) was determined by the balance

https://doi.org/10.5194/bg-2019-366
Preprint. Discussion started: 18 November 2019

between incoming and outgoing radiation components:

$$Rn_x = Rsn_{b,x} + Rsn_{d,x} + Rln_x \quad \text{(A7)}$$

where $Rsn_{b,x}$ and $Rsn_{d,x}$ are the absorbed energy from direct and diffuse radiation; Rln_x is the absorbed net longwave radiation.

Algorithms for calculating the net radiation components were detailed in Gong et al. (2013), as modified from the methods of Chen et al. (1999). Canopy light interception was determined by the light-extinction coefficient (k_{light}), leaf area index (Lc) and solar zenith angle. The partitioning of reflected and absorbed irradiances at ground surface was regulated by the surface albedos for the shortwave (a_s) and longwave (a_l) components, and the temperature of surface x (T_x) also affects net longwave radiation:

$$Rn_x = Rsn_{b,x} + Rsn_{d,x} + Rln_x \quad \text{(A8)}$$

$$Rsn_{d,x} = Rs_{id,x}(1 - a_s) \quad \text{(A9)}$$

$$Rln_x = Rl_{i,x}(1 - a_l) - \varepsilon\delta T_x^4 \quad \text{(A10)}$$

where Rs_{ib}, Rs_{id}, Rl_i are the incoming beam, diffusive and longwave radiations; ε is the emissivity ($\varepsilon = 1-a_l$); δ is the Stefan Boltzmann's constant (5.67×10^{-8} W m^{-2} K^{-4}).

Rn_x was partitioned into latent heat flux (λE_x), sensible heat flux (H_x) and ground heat flux (for canopy G_1=0):

$$Rn_x = H_x + \lambda E_x + G_x \quad \text{(A11)}$$

$$G_1 = K_T\,(T_x - Ts)/(0.5z) \quad \text{(A12)}$$

where Ts is the temperature of the moss carpet; z is the thickness of the moss layer (z = 5 cm).

The latent heat flux was calculated by the "interactive scheme" (Daamen and McNaughton, 2000; see also in Gong et al., 2016), which is a K-theory-based, multi-source model:

$$\lambda E_x = \frac{(\Delta/\gamma)A_x r_{sa,x} + \lambda VPD_b}{r_{b,x} + (\Delta/\gamma) r_{sa,x}} \quad \text{(A13)}$$

where Δ is the slope of the saturated vapor pressure curve against air temperature; λ is the latent heat of vaporization; E is the evaporation rate; VPD_b is the vapor pressure deficit at z_b; $r_{b,x}$ is the total resistance to water vapor flow, the sum of boundary layer resistance ($r_{sa,x}$) and surface resistance (r_{ss}); and A is the available energy for evapotranspiration and $A_x = Rn_x - G_x$.

The calculations of γ, λ and VPD_b require the temperature (T_b) and vapor pressure (e_b) at the mean source height (z_b). These variables were related to the total of latent heat ($\sum\lambda E_x$) and sensible heat ($\sum H_x$) from all surfaces using the Penman-type equations:

$$\Sigma\lambda E_x = \rho_a C_p\,(e_b - e_a)/(r_{aero}\gamma) \quad \text{(A14)}$$

$$\Sigma H_x = \rho_a C_p\,(T_b - T_a)/r_{aero} \quad \text{(A15)}$$

where $\rho_a C_p$ is the volumetric specific heat of air; r_{aero} is the aerodynamic resistance between z_b and the

https://doi.org/10.5194/bg-2019-366
Preprint. Discussion started: 18 November 2019

reference height z_a, and was a function of T_b accounting for the atmospheric stability (Choudhury and Monteith, 1988); and γ is the psychrometric constant ($\gamma=\rho_a Cp/\lambda$).

Changes in the energy balance affect the surface temperature (T_x) and vapor pressure (e_x), which further feed back to the energy availability (Eq. A10, A12), the source-height temperature, *VPD* and the resistance parameters (e.g., r_{aero}). The values of T_x and e_x were solved iteratively by coupling the energy balance equations (eqs. A11–A15) with the Penman-type equations (see also Appendix B in Gong et al., 2016):

$$\lambda E_x = \rho_a C_p (e_x - e_b)/(r_{sa,x}\gamma) \quad \text{(A16)}$$

$$H_x = \rho_a C_p (T_x - T_b)/r_{sa,x} \quad \text{(A17)}$$

where the boundary-layer resistance for ground surface ($r_{sa,1}$) and canopy ($r_{sa,0}$) were calculated following the approaches of Choudhury and Monteith (1988).

Sink terms of transport functions for water and heat

The sink term $S_{h,i}$ (see Eq. A11) for each soil layer i was calculated as:

$$S_{h,i} = E_i - P_i - W_{melt,i} - I_i \quad \text{(A18)}$$

where E_i is the evaporation loss of water from the layer; P_i is rainfall (P_i = 0 if the layer is not topmost, i.e. i>1); $W_{melt,i}$ is the amount of melt water added to the layer; I_i is the net water inflow and was calibrated in Section 2.5.

The value of E_i was calculated as:

$$E_i = f_{top}E_0 + f_{root}(i)E_1 \quad \text{(A19)}$$

where E_0 and E_1 are the evaporation rate from ground surface and canopy (Eq. A13); f_{top} is the location multiplier for the topmost layer (f_{top} = 0 in cases i>1); and $f_{root}(i)$ is the fraction of fine-root biomass in layer i.

The value of $W_{melt,i}$ was controlled by the freeze-thaw dynamics of soil water and snow pack, which were related to the heat diffusion in soil profile (Eq. A2). We set the freezing point temperature to 0 ºC, and the temperature of a soil layer was held constant (0 ºC) during freezing or melting. For the ith soil layer, the sink term (S_T) in heat transport equation (Eq. A2) was calculated as:

$$S_{T,i} = f_{phase}max(|T_i|C_{T,i}, W_{phase}\lambda_{melt}) \quad \text{(A20)}$$

where $C_{T,i}$ is specific heat of soil layer (Eq. A13); W_{phase} is the water content for freezing ($W_{phase} = \theta_w$) or melting ($W_{phase} = \theta_{ice}$); λ_{melt} is the latent heat of freezing; f_{phase} is binarial coefficient that denotes the existence of freezing or thawing. For each time step t, we computed $T_i(t)$ with a piror assumption that $S_{T,i}$=0. Then f_{phase} was determined by whether the temperature changed across the freezing point, i.e. f_{phase}=1 if $T_i(t)*T_i(t-1) \leq 0$, otherwise f_{phase}= 0.

https://doi.org/10.5194/bg-2019-366
Preprint. Discussion started: 18 November 2019

Biogeosciences Discussions Open Access EGU

Appendix B. Methods and results of the empirical study on *Sphagnum* capitula water retention as a controlling mechanism for peatland moss community dynamics

Measurement of morphological traits

To quantify morphological traits, samples of *S. fallax* and *S. magellanicum* were collected at the end of August 2016 with a core (size d 7cm, area 50 cm^2, height at least 8 cm) maintaining the natural density of the stand. Samples were stored in plastic bags at cool room (4 ºC) until measurements. Eight replicates were collected for each species. For each sample, capitulum density (D_S, shoots cm^{-2}) was measured and ten moss shoots were randomly selected and separated into capitula and stems (5 cm below capitula). The capitula and stems were moistened and placed on top of a tissue paper for 2 minutes to extract free-moving water, before weighing them for water-filled fresh weight. The samples were dried at 60 °C for at least 48h to measure the dry masses. The field-water contents of capitula (W_{cf}, g g^{-1}) and stems (W_{sf}, g g^{-1}) were then calculated as the ratio of water to dry mass for each sample. The biomass of capitula (B_{cap}, g m^{-2}) and living stems (B_{st}, g m^{-2}) were calculated by multiplying the dry masses with the capitulum density (D_S). Biomass density of living stems (H_{spc}, g cm^{-1} m^{-2}) was calculated by dividing B_{st} with the length of stems.

Measurement of photosynthetic traits

We measured the photosynthetic light response curves for *S. fallax* and *S. magellanicum* with fully controlled, flow-through gas-exchange fluorescence measurement systems (GFS-3000, Walz, Germany; Li-6400, Li-Cor, US) under varying light levels. In 2016, measurements on field-collected samples were done during May and early June, which is a peak growth period for *Sphagna* (Korrensalo et al. 2017). Samples were collected from the field site each morning and were measured the same day at Hyytiälä field station. Samples were stored in plastic containers and moistened with peatland water to avoid changes in plant status during the measurement. Right before the measurement we separated *Sphagnum* capitula from their stems and dried them lightly using tissue paper before placing them in a custom-made cuvette (Korrensalo et al. 2017). Net photosynthesis rate (A, µmol m^{-2} s^{-1}) was measured at 1500, 250, 35, and 0 µmol m^{-2} s^{-1} photosynthetic photon flux density ($PPFD$). The samples were allowed to adjust to cuvette conditions before the first measurement and after each change in the PPFD level until the CO_2 rate had reached a steady level, otherwise the cuvette conditions were kept constant (temperature 20°C, CO_2 concentration 400 ppm, relative humidity of inflow air 60%, flow rate 500 umol s^{-1} and impeller at level 5). The time required for a full measurement cycle varied between 60 and 120 minutes. Each sample was weighed before and after the gas-exchange measurement, then dried at 40°C for 48 h to determine the biomass of capitula (B_{cap}). For each species, four samples were measured as replicates and were made to fit a hyperbolic light-saturation curve (Larcher, 2003):

$$A_{20} = \left(\frac{Pm_{20} * PPFD}{\alpha_{PPFD} + PPFD} - Rs_{20}\right) * B_{cap} \quad \text{(B1)}$$

where subscript 20 denotes the variable value measured at 20 °C; Rs is the mass-based dark respiration rate (µmol g^{-1} s^{-1}); Pm is the mass-based rate of maximal gross photosynthesis (µmol g^{-1} s^{-1}); and α_{PPFD} is the half-saturation point (µmol m^{-2} s^{-1}), i.e., PPFD level where half of Pm is reached. The measured morphological and photosynthetic traits are listed in Table 1.

https://doi.org/10.5194/bg-2019-366
Preprint. Discussion started: 18 November 2019

991

992 *Drying experiment*

993 To link the water retention and photosynthesis of *Sphagnum* capitula, we performed a drying experiment
994 using a GFS-3000 system to measure co-variations of capitulum water potential (*h*, cm water), water content
995 (W_{cap}, g g^{-1}) and *A* (μmol m^{-2} g^{-1} s^{-1}). For both species, four mesocosms were collected in August 2018 and
996 transported to laboratory in UEF Joensuu, Finland. Capitula were harvested and wetted by water from the
997 mesocosms. The capitula were then placed gently on a piece of tissue paper for 2 minutes and then placed
998 into the same cuvette as used in the previous photosynthesis measurement. The cuvette was then placed
999 into GFS and measured under constant conditions of *PPFD* (1500 umol m-2 s-1), temperature (293.2K),
1000 inflow air (700 umol s-1), CO_2 concentration (400 ppm) and relative humidity (40%). Measurement was
1001 stopped when *A* dropped to less than 10% of its maximum. Each measurement lasted between 120 and180
1002 minutes. Each sample was weighed before and after the gas-exchange measurement, then dried at 40°C for
1003 48 h to determine the biomass of capitula (B_{cap}).

1004 The GFS-3000 records the vapor pressure (e_a, kPa) and the evaporation rate (*E*, g s^{-1}) simultaneously with
1005 *A* at one hertz (Heinz Walz GmbH, 2012). The changes in W_{cap} with time (*t*) was calculated as following:

1006 $$RWC(t) = \left(W_{pre} - B_c - \sum_{t=0}^{t} E(t)\right)/B_c \quad \text{(B2)}$$

1007 We assumed that the vapor pressure at the surface of water-filled cells equaled the saturation vapor
1008 pressure (e_s), and the vapor pressure in the headspace of cuvette equaled that in the outflow (e_a). The vapor
1009 pressure in capitula pores (e_i) thus can be calculated based on following gradient-transport function (Fig.
1010 B1A):

1011 $$\lambda E(t) = \frac{\rho_a C_p}{\gamma} \frac{(e_i(t) - e_a(t))}{r_a(t)} = \frac{\rho_a C_p}{\gamma} \frac{(e_s - e_i(t))}{r_s(t)} \quad \text{(B3)}$$

1012 where λ is the latent heat of vaporization; γ is the slope of the saturation vapor pressure - temperature
1013 relationship; r_a is the aerodynamic resistance (m s^{-1}) for vapor transport from inter-leaf volume to
1014 headspace; r_s is the surface resistance of vapor transport from wet leaf surface to inter-leaf volume. The
1015 bulk resistance for evaporation (r_{bulk}) was thus calculated as r_a+r_s.

1016 We assumed that the structures of tissues and pores did not change during the drying process and assumed
1017 r_a to be constant during each measurement. *A* tended to increase with time *t* until it peaked (A_m) and then
1018 decreased (Fig. 1B). The point A=A_m implied the water content where further evaporative loss would start
1019 to drain the cytoplasmic water, leading to the decrease in *A*. The response of *A* to W_{cap} was fitted as a
1020 second-order polynomial function (Robroek et al., 2009) using data from t_{Am} to t_n:

1021 $$f_A(W_{cap}) = a_{W0} + a_{W1} * W_{cap} + a_{W2} * W_{cap}^2 \quad \text{(B4)}$$

1022 where a_{W0}, a_{W1} and a_{W2} are parameters; and $f_A(W_{cap}) = A/A_m$. For each replicate, the optimal water content
1023 for photosynthesis (W_{opt}) was derived from the peak of fitted curve (Eq. 4). The capitulum water content at
1024 the compensation point W_{cmp}, where the rates of gross photosynthesis and respiration are equal, can be
1025 calculated from the point A=0.

https://doi.org/10.5194/bg-2019-366
Preprint. Discussion started: 18 November 2019

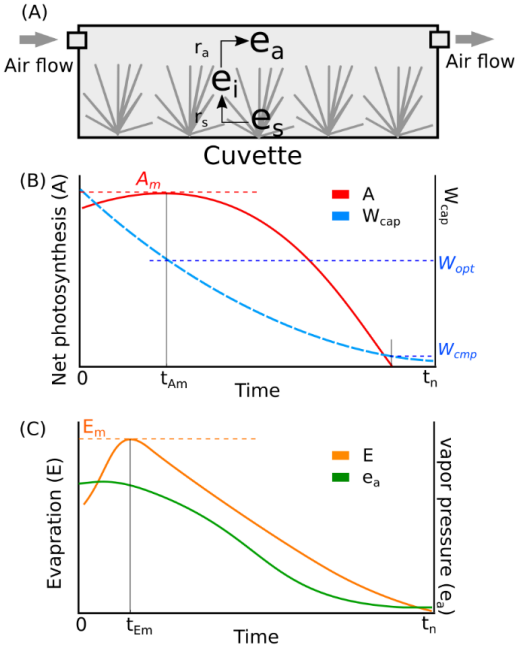

Figure B1. Conceptual schemes of (A) cuvette setting and resistances, (B) the co-variations of net photosynthesis and W_{cap}, and (C) the co-variations of evaporation and vapor pressure in headspace during a measurement. Meanings of symbols: e_a, vapor pressure in headspace of cuvette (kPa); e_i, vapor pressure in branch-leaf structure of capitula; e_s, vapor pressure at the surface of wet tissues; r_a, aerodynamic resistance of vapor diffusion from inner capitula to headspace; r_s, surface resistance of vapor diffusion from wet tissue surface to inner capitula space; A, net photosynthesis rate (µmol m^{-2} s^{-1}); A_m, maximal net photosynthesis rate (µmol m^{-2} s^{-1}); W_{cap}, water content of capitula (g g^{-1}); W_{opt}, W_{cap} at A=A_m; W_{cmp}, W_{cap} at A=0; E, evaporation rate (mm s^{-1}).

Similarly, the evaporation rate (E) increased from the start of measurement until maximum evaporation E_m, and then decreased (Fig. B1C). The point E=E_m implied the time when the wet capitulum tissues were maximally exposed to the air flow. Therefore, r_a was estimated as the minimum of bulk resistance using Eq. (B5), by assuming $e_i(t)$≈e_s when $E(t)$ = E_m:

$$r_a = \frac{\rho_a C_p}{\gamma} \frac{(e_s - e_a(t))}{\lambda E_m} \quad \text{(B5)}$$

Based on the calculated $e_i(t)$, we were able to derive the capitulum water potential (h) following the equilibrium vapor-pressure method (e.g. Price et al, 2008; Goetz and Price, 2015):

$$h = \frac{RT}{Mg} ln\left(\frac{e_i}{e_s}\right) + h_0 \quad \text{(B6)}$$

where R is the universal gas constant (8.314 J mol^{-1} K^{-1}); M the molar mass of water (0.018 kg mol^{-1}); g is the gravitational acceleration (9.8 N kg^{-1}); e_i/e_s is the relative humidity; h_0 is the water potential due to the emptying of free-moving water before measurement (set to 10 kPa according to Hayward and Clymo, 1982).

Statistical analysis

The light response curve (Eq. B1) and the response function of A/A_m to W_{cap} changes (Eq. B4) were fitted using nlme package in R Studio (version 3.1). The obtained values of shape parameters a_{W0}, a_{W1} and a_{W2} (Eq. 4) were then used to calculate W_{opt} (W_{opt} = -0.5 a_{W1}/ a_{W2}) and W_{cmp} (W_{cmp} = 0.5 [-a_{W1} - (a_{W1}^2 - 4a_{W0}

https://doi.org/10.5194/bg-2019-366
Preprint. Discussion started: 18 November 2019

Biogeosciences Discussions Open Access EGU

$a_{W2})^{0.5}] / a_{W2}$). We then applied ANOVA to compare *S. magellanicum* against *S. fallax* for the traits obtained from the field sampling (i.e. structural properties such as B_{cap}, D_S, H_{spc}, W_{cf}, W_{sf}) and from the gas-exchange measurements (i.e. Pm_{20}, Rs_{20}, W_{opt}, W_{cmp} and r_{bulk}), using R Studio (version 3.1).

The measured values of capitulum water potential (h) were $\log_{10}$-transformed and related to the variations in W_{cap}, B_{cap} and D_S with a linear model. Similarly, a linear model was established to quantify the response of bulk resistance for evaporation (r_{bulk}) ($\log_{10}$-transformed) to the variations in h, B_{cap} and D_S. The linear regressions were based on statsmodels (version 0.9.0) in Python (version 2.7), as supported by Numpy (version 1.12.0) and Pandas (version 0.23.4) packages.

Results of the empirical measurements

The two *Sphagnum* species differed in their structural properties (Table B1). Lawn species S. *fallax* had looser structure than hummock species *S. magellanicum* as seen in lower capitulum density (D_S) and specific height (H_{spc}) in *S. fallax* than in *S. magellanicum* ($P<0.05$, Table. B1). Moreover, in conditions prevailing in the study site *S. fallax* mosses were dryer than *S. magellanicum*; the field-water contents of *S. fallax* capitulum (W_{cf}) and stem (W_{sf}) were 40% and 46% lower than *S. magellanicum* ($P<0.01$, Table. B1), respectively. The different density of capitulum of the two species differing in their capitulum size led to similar capitulum biomass (B_{cap}) ($P=0.682$) between *S. fallax* with small capitulum and *S. magellanicum* with large capitulum. Unlike the structural properties, maximal CO_2 exchange rates (Pm_{20} and Rs_{20}) did not differ between the two species (Table B1).

The drying experiment demonstrated how capitulum water content regulated capitulum processes in both studied *Sphagnum* species (Fig. B2). Decreasing capitulum water content (W_{cap}) led to decrease in the water potential (h), the responses of h to W_{cap} varied among replicates (Fig. 2A). The values of W_{cap} for *S. fallax* were generally lower than those for *S. magellanicum* under the same water potentials. The fitted linear models explained over 95% of the variations in the measured h for both species (Table. B2), although fitted responses of h to W_{cap} were slightly smoother than the measured ones, particularly for *S. magellanicum* (Fig. B2A). The responses of h to W_{cap} was significantly affected by the capitulum density (D_S), capitulum biomass (B_{cap}) and their interactions with W_{cap} (Table. B2).

Decreasing capitulum water content (W_{cap}), and water potential (h), were associated with increasing bulk resistance for evaporation (r_{bulk}, Fig. B2B), although the sensitivity of r_{bulk} to h changes varied by replicates. The values of r_{bulk} from *S. fallax* were largely lower than those from *S. magellanicum* when the capitulum water content of the two species were similar. The fitted linear models explained the observed variations in the measured r_{bulk} well for both species (Fig. 2B and Table. B3). The variation in the response of r_{bulk} to h was significantly affected by capitulum density (D_S), capitulum biomass (B_{cap}) and their interactions with h (Table. B3).

Decreasing capitulum water content (W_{cap}) slowed down the net photosynthesis rate (Fig. B2C), as represented by the decreasing ratio of A/A_m. *S. fallax* required lower capitulum water content (W_{cap}) than *S. magellanicum* to reach photosynthetic maximum and photosynthetic compensation point. However, the ranges of capitulum water content from photosynthetic maximum (W_{opt}) or field capacity (W_{fc}) to that at compensation point (W_{cmp}) were smaller for *S. fallax* than *S. magellanicum*. Hence, *S. fallax* had narrower

https://doi.org/10.5194/bg-2019-366
Preprint. Discussion started: 18 November 2019

transition zone for photosynthesis to respond to drying, compared to *S. magellanicum*.

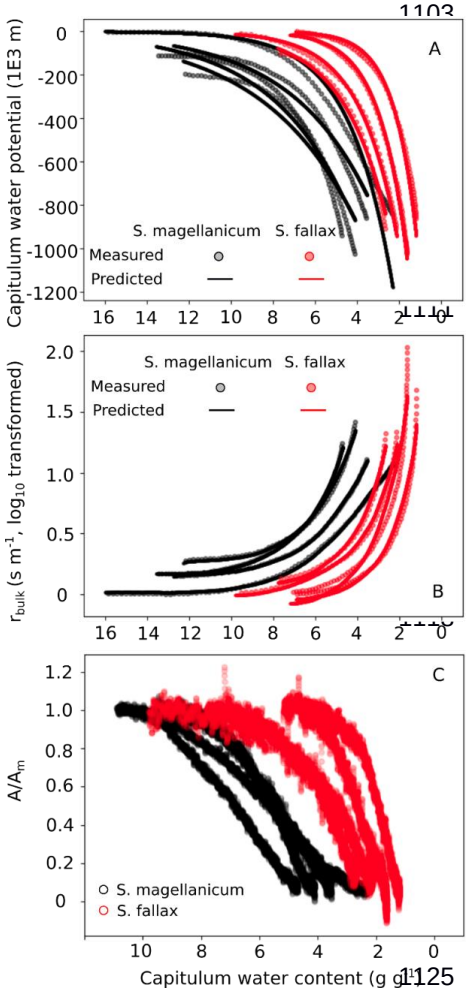

Figure B2. Responses of (A) capitulum water potential, (B) bulk resistance of evaporation, and (C) net photosynthesis to changes in capitulum water content (W_{cap}) of two *Sphagnum* species typical to hummocks (*S. magellanicum*, black) and lawns (*S. fallax*, red). As the measured results are based on the drying experiment starting with fully wetted capitula characteristic for both species, the X-axis is shown from high to low W_{cap}. The values predicted in (B) and (C) are based on linear models with parameter values listed in Tables 2 and 3 and predictor values from the drying experiment.

https://doi.org/10.5194/bg-2019-366
Preprint. Discussion started: 18 November 2019

Biogeosciences Discussions Open Access EGU

Table. B1 Species-specific traits of morphological, photosynthetic and water-retention from *S. magellanicum* and *S. fallax*. Trait values (mean ± standard deviation) and ANOVA statistics F- and p-values are given for comparing the means of traits of the two species.

Trait	*S. magellanicum*	*S. fallax*	F	P (>F)
Capitulum density, D_S (capitula cm^{-2})	0.922±0.289	1.46±0.323	6.224[a]	0.037 *
Capitulum biomass, B_{cap} (g m^{-2})	75.4±21.5	69.2±19.6	0.181[a]	0.682
Specific height, H_{spc} (cm g^{-1} m^{-2})	45.4 ± 7.64	32.6±6.97	6.126[a]	0.038*
Field water content of capitula, W_{cf} (g g^{-1})	14.7±3.54	8.09±1.48	11.75[a]	0.009**
Field water content of stems, W_{sf} (g g^{-1})	18.4±1.92	10.2±1.50	45.81[a]	0.0001**
Maximal gross photosynthesis rate at 20 ºC, Pm_{20} (µmol g^{-1} s^{-1})	0.019±0.004	0.014±0.002	3.737[b]	0.101
Respiration rate at 20 ºC, Rs_{20} (µmol g^{-1} s^{-1})	0.007±0.004	0.007±0.002	0.012[b]	0.92
half-saturation point of photosynthesis, α_{PPFD} (µmol g^{-1} s^{-1})	101.4±14.1	143±51.2	2.856[b]	0.142
Optimal capitulum water content for photosynthesis, W_{opt} (g g^{-1})	9.41±0.73	5.81±1.68	11.57[b]	0.0145*
Capitulum water content at photosynthetic compensation point, W_{cmp} (g g^{-1})	3.67±0.83	1.78±0.43	12.35[b]	0.0126*
Minimal bulk resistance of evaporation, r_a (m s^{-1})	33.5±7.30	40.7±4.99	1.976[b]	0.2165

[a] soil-core measurement, sample n=5; [b] cuvette gas-exchange measurement, sample n=4; * the difference of means is significant (P<0.05); ** the difference of means is very significant (P<0.01).

Table B2. Parameter estimates of the linear model for the $\log_{10}$-transformed capitulum water potential (h) for *S. fallax* and *S. magellanicum*. Estimate value, standard error (SE), and test statistics p-values are given to the predictors of the models. Predictors are: capitulum biomass (B_{cap}), capitulum density (D_S), capitulum water content (W_{cap}), the interaction of capitulum biomass and water potential (B_{cap}×W_{cap}), the interactions of capitulum biomass and capitulum density (D_S×W_{cap}), the interactions of capitulum density and water potential (D_S×W_{cap}), and the interaction of capitulum biomass, capitulum density and water potential (B_{cap}×D_S× W_{cap}). All coefficient values are significantly different from 0 (p<0.001).

Parameter	*S. magellanicum* (R^2=0.972)		*S. fallax* (R^2=0.984)	
	Value	SE	Value	SE
(Intercept)	25.30	0.253	-90.99	2.158
B_{cap}	-272.10	3.133	2294.67	52.342
W_{cap}	-9.50	0.031	-62.12	0.600
B_{cap}×W_{cap}	114.61	0.387	1500.26	14.549
D_S	-21.76	0.253	104.11	2.376
B_{cap}×D_S	268.95	3.112	-2422.79	55.251
D_S×W_{cap}	9.33	0.031	68.35	0.661
B_{cap}×D_S×W_{cap}	-113.33	0.386	-1588.06	15.360

https://doi.org/10.5194/bg-2019-366
Preprint. Discussion started: 18 November 2019

Biogeosciences Discussions Open Access EGU

Table B3. Parameter estimates of the linear model for the $\log_{10}$-transformed capitulum evaporative resistance (r_{bulk}) for *S. fallax* and *S. magellanicum*. Estimate value, standard error (SE), and test statistics p-values are given to the predictors of the models. Predictors are: capitulum biomass (B_{cap}), capitulum density (D_S), water potential (h), the interaction of capitulum biomass and water potential ($B_{cap}\times h$), the interactions of capitulum biomass and capitulum density ($D_S\times h$), the interactions of capitulum density and water potential ($D_S\times h$), and the interaction of capitulum biomass, capitulum density and water potential ($B_{cap}\times D_S\times h$). All coefficient values are significantly different from 0 ($p<0.001$).

Parameter	*S. magellanicum* (R^2=0.998)		*S. fallax* (R^2=0.966)	
	Value	SE	Value	SE
(Intercept)	-1.13	0.027	55.07	2.225
B_{cap}	14.45	0.334	1334.55	53.968
h	0.0012	5.92e-05	-0.028	0.004
$B_{cap}\times h$	-0.0007	0.001	0.707	0.101
D_S	1.08	0.027	-60.53	2.450
$B_{cap}\times D_S$	-13.39	0.333	1406.36	56.968
$D_S\times h$	0.0002	5.89e-05	0.0317	0.005
$B_{cap}\times D_S\times h$	-0.0017	0.001	-0.733	0.106

References

Goetz, J. D. and Price, J. S.: Role of morphological structure and layering of *Sphagnum* and *Tomenthypnum* mosses on moss productivity and evaporation rates, Canadian Journal of Soil Science, 95, 109-124, 2015.

Hayward P. M. and Clymo R. S.: Profiles of water content and pore size in Sphagnum and peat, and their relation to peat bog ecology. Proceedings of the Royal Society of London, Series B, Biological Sciences, 215, 299-325, 1982.

Korrensalo, A., Alekseychik, P., Hájek, T., Rinne, J., Vesala, T., Mehtätalo, L., Mammarella, I. and Tuittila, E.-S.: Species-specific temporal variation in photosynthesis as a moderator of peatland carbon sequestration, Biogeosciences, 14, 257-269, 2017.

Larcher, W.: Physiological Plant Ecology: Ecophysiology and Stress Physiology of Functional Groups, Springer, 2003.

Price, J. S., Whittington, P. N., Elrick, D. E., Strack, M., Brunet, N. and Faux, E.: A method to determine unsaturated hydraulic conductivity in living and undecomposed moss, Soil Sci. Soc. Am. J., 72, 487 – 491, 2008.

Robroek, B. J.M., Schouten, M. G.C., Limpens, J., Berendse, F. and Poorter, H.: Interactive effects of water table and precipitation on net CO_2 assimilation of three co-occurring Sphagnum mosses differing in distribution above the water table, Global Change Biology 15, 680 – 691, 2009.

https://doi.org/10.5194/bg-2019-366
Preprint. Discussion started: 18 November 2019

Appendix C. Comparisons of meteorological variables simulated by Weather Generator and those measured from Siikaneva peatland site (ICOS site located in 10 km distance from the study site Lakkasuo)

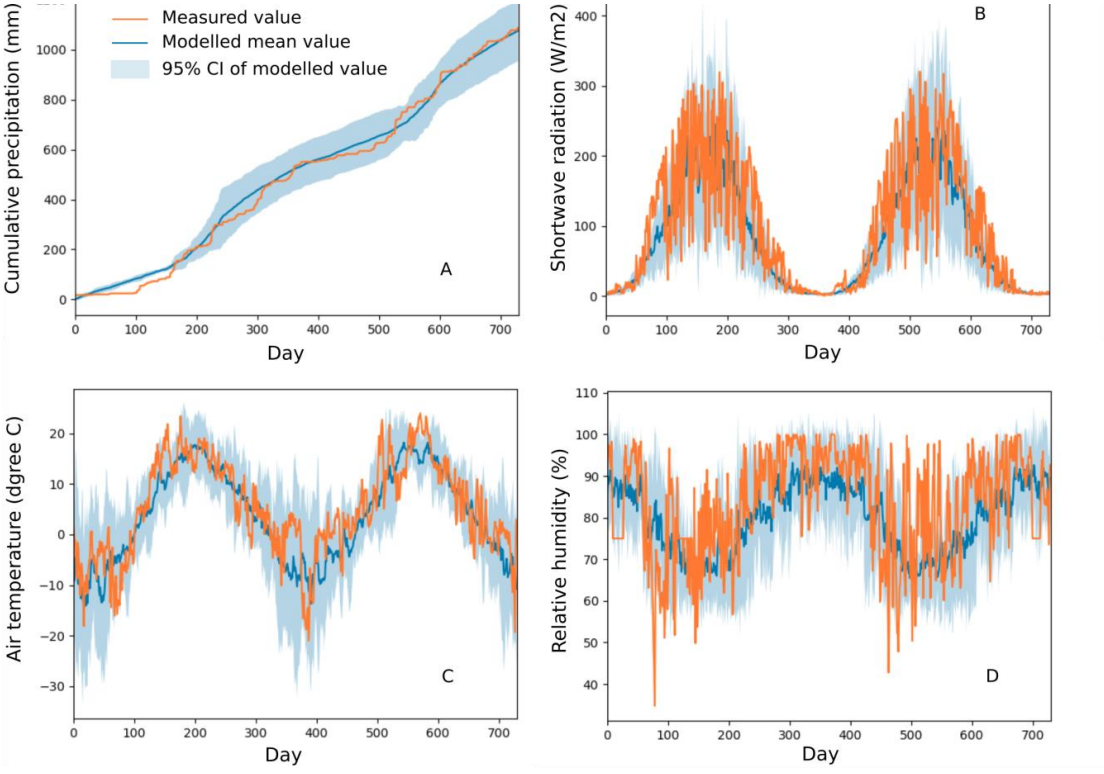

Fig. C1 Comparisons of meteorological variables simulated by Weather Generator and those measured from Siikaneva peatland site. The variables include (A) cumulative precipitation (mm), (B) incoming shortwave radiation (W m^{-2}), (C) air temperature (°C), and (D) relative humidity (%). These variables were measured and simulated at half-hourly timescale. The measurements were carried out during 2012-2013. Details about the site and measurements have been described by Alekseychik et al. (2018). The measured seasonal dynamics of the meteorological variables were generally in line with the 95% confidence intervals (CI) of the simulated values, which were calculated based on Monte-Carlo simulations (n=5).

https://doi.org/10.5194/bg-2019-366
Preprint. Discussion started: 18 November 2019

Biogeosciences Discussions Open Access EGU

1178 **Appendix D. Comparisons of seasonal water table measured from the study site and the values**
1179 **simulated based on calibrated net inflow**

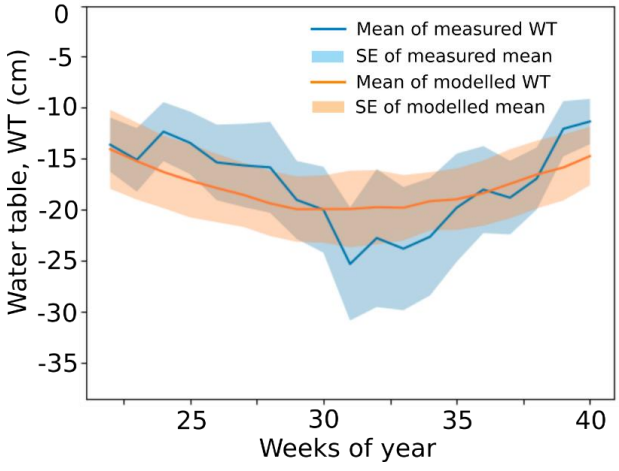

1180

1181 Fig. D1 Comparison of seasonal water table (WT) measured at the Lakkasuo study site and the values
1182 simulated by the calibrated PCS. WT values were sampled weekly from the lawn habitats both in field and
1183 in model output. The weekly mean WT was measured during 2001, 2002, 2004 and 2016. The modelled
1184 means and standard deviations (SD) of WT were based on 20 Monte-Carlo simulations. The simulated
1185 seasonality of mean WT generally followed the measured trends. The calibration reduced the sum of
1186 squared error (*SE*, Eq. 12) from 199.5 (a_N=b_N=0) to 117.3. The calibrated values for a_N and b_N were -
1187 $5.3575*10^{-4}$ and $4.7599*10^{-5}$, respectively (Eq. A18).